

# Redshift-distance Survey of Early-type Galaxies: The $D_n - \sigma$ Relation <sup>1</sup>

M. Bernardi<sup>1</sup>, M. V. Alonso<sup>2</sup>, L. N. da Costa<sup>3,4</sup>, C. N. A. Willmer<sup>4,5</sup>

G. Wegner<sup>6</sup>, P. S. Pellegrini<sup>4</sup>, C. Rit  <sup>4</sup>, M. A. G. Maia<sup>4</sup>

## ABSTRACT

In this paper  $R$ -band photometric and velocity dispersion measurements for a sample of 452 elliptical and S0 galaxies in 28 clusters are used to construct a template  $D_n - \sigma$  relation. This template relation is constructed by combining the data from the 28 clusters, under the assumption that galaxies in different clusters have similar properties. The photometric and spectroscopic data used consist of new as well as published measurements, converted to a common system, as presented in a accompanying paper. The resulting direct relation, corrected for incompleteness bias, is  $\log D_n = 1.203 \log \sigma + 1.406$ ; the zero-point has been defined by requiring distant clusters to be at rest relative to the CMB. This zero-point is consistent with the value obtained by using the distance to Virgo as determined by the Cepheid period-luminosity relation. This new  $D_n - \sigma$  relation leads to a peculiar velocity of  $-72 \pm 189 \text{ kms}^{-1}$  for the Coma cluster. The scatter in the distance relation corresponds to a distance error of about 20%, comparable to the values obtained for the Fundamental Plane relation. Correlations between the scatter and residuals of the  $D_n - \sigma$  relation with other parameters that characterize the cluster and/or the galaxy stellar population are also analyzed. The direct and inverse relations presented here have been used in recent studies of the peculiar velocity field mapped by the ENEAR all-sky sample.

*Subject headings:* cosmology: observations – galaxies: large-scale structure – galaxies: clustering

---

<sup>1</sup>The University of Chicago, 5640 South Ellis Avenue, Chicago, IL 60637, USA

<sup>2</sup>Observatorio Astronómico de Córdoba, Laprida 854, Córdoba, 5000, Argentina

<sup>3</sup>European Southern Observatory, Karl-Schwarzschild Strasse 2, D-85748 Garching, Germany

<sup>4</sup>Departamento de Astronomia, Observatório Nacional, Rua Gen. José Cristino 77, Rio de Janeiro, R.J., 20921, Brazil

<sup>5</sup>UCO/Lick Observatory, University of California, 1156 High Street, Santa Cruz, CA 95064, USA

<sup>6</sup>Department of Physics & Astronomy, Dartmouth College, Hanover, NH 03755-3528, USA

<sup>1</sup>Based on observations at Complejo Astronomico El Leoncito (CASLEO), operated under agreement between the Consejo Nacional de Investigaciones Cientificas de la República Argentina and the National Universities of La Plata, Córdoba and San Juan; Cerro Tololo Interamerican Observatory (CTIO), operated by the National Optical Astronomical Observatories, under AURA; European Southern Observatory (ESO), partially under the ESO-ON agreement; Fred Lawrence Whipple Observatory (FLWO); Observatório do Pico dos Dias, operated by the Laboratório Nacional de Astrofísica (LNA); and the MDM Observatory on Kitt Peak.

## 1. Introduction

Present-day elliptical galaxies form a remarkably homogeneous class of objects which obey scaling relations involving their structural and dynamical properties. Indeed, elliptical galaxies are known to populate the so-called fundamental plane (FP, Djorgovski & Davis 1987; Dressler et al. 1987), in a three-dimensional space defined by the surface brightness  $\mu_e$ , the effective radius  $r_e$ , and internal velocity dispersion  $\sigma$ . Therefore, by choosing an appropriate combination of parameters, a tight relation between distance-dependent and independent quantities can be found; the  $D_n - \sigma$  relation is such a relation (Dressler et al. 1987), where  $D_n$  is the physical scale of the galaxy defined at a specified surface brightness level ( $D_n \equiv d_n \times R$ , where  $d_n$  is a measure of the angular size of the galaxy and  $R$  is the distance of the galaxy). The existence of such scaling relations provides an important tool for studying the properties of the stellar populations and the evolution of ellipticals (e.g., Jørgensen, Franx, & Kjørgaard 1996; Franx et al. 1997), and for constraining models of spheroidal formation (e.g., Bressan, Chiosi, & Fagotto 1994; Baugh, Cole, & Frenk 1996). Furthermore, these relations provide the means of measuring relative distances to early-type galaxies. This is the primary goal of this work. At the present time, some doubts remain whether these relations depend on the environment (e.g., Gibbons, Fruchter, & Bothun 2001); if they do, this would lead to the measurement of spurious motions. Also, until recently, it was unclear how distances derived using  $D_n - \sigma$  related to those measured by the Tully-Fisher relation (Scodeggio 1997; Scodeggio, Giovanelli, & Haynes 1997).

The FP and the  $D_n - \sigma$  scaling relations are not entirely equivalent (Jørgensen, Franx, & Kjørgaard 1993) and the  $D_n - \sigma$  relation is expected to be less accurate if the range of galaxy sizes is large (Kelson et al. 2000). In addition, it has been claimed that the scatter around the FP is smaller, suggesting that  $D_n - \sigma$  distances are less accurate (Jørgensen et al. 1993). However, recent studies do not seem to support these claims (Jørgensen et al. 1996; D’Onofrio et al. 1997; Hudson et al. 1997). While the FP relation is usually used for detailed cluster studies, for large samples such as the magnitude-limited, all-sky sample of early-type galaxies (ENEAR, da Costa et al. 2000a) presented below, the number of galaxies with available  $d_n$  measurements is  $\sim 50\%$  larger than the number with available FP measurements. Therefore, since the primary goal of this project has been to estimate galaxy distances and derive the peculiar velocity field, we have focused our attention on the derivation of a template  $D_n - \sigma$  relation. A similar analysis for the FP relation will be presented in a future paper.

This work uses the ENEARc sample of early-type galaxies in 28 clusters presented by Bernardi et al. (2001; hereafter B01). This sample combines data available in the literature with new measurements converted into a common system thanks to the effort of securing new measurements for a large number of galaxies in common with previously available samples. Another important feature of the sample is that cluster membership was carried out using groups identified in complete redshift surveys of the nearby universe, thereby leading to a more systematic assignment than was possible in earlier work.

In this paper we obtain  $D_n - \sigma$  fits for each of the 28 clusters accounting for various possible biases. We then combine the sample to construct a global template relation under the assumption that early-type galaxies in different clusters are similar. We also study the residuals with respect to the template to investigate, a posteriori, the accuracy of this assumption. The resulting relation is used to compute peculiar velocities of clusters as well as of the ENEAR all-sky sample of early-type galaxies. Both these samples have been used to measure the bulk flow velocity, to set constraints on cosmological parameters and to characterize the velocity field and mass distribution in the local universe (da Costa et al. 2000b; Borgani et al. 2000b; Nusser et al. 2001; Zaroubi et al. 2001).

The paper is organized as follows: in Section 2 the data set with the individual galaxy parameters is

described. In Section 3 we present the calibration of the direct (forward)  $D_n - \sigma$  relation. We quantify the selection bias which, if not corrected for, can lead to an erroneous determination of the distance relation coefficients and its scatter. This is critical for studies of the cosmic flow field and the properties of early-type galaxies. The direct relation has been applied to compute distances for the galaxy sample used in da Costa et al. (2000b) and Zaroubi et al. (2001). Also shown are the parameters for the inverse relation obtained by regressing on the distance-independent quantity  $\log(\sigma)$ ; this inverse relation has been used in the analysis of the peculiar velocity field of clusters and “field” galaxies in redshift space (Borgani et al. 2000b; Nusser et al. 2001). The measured distances and peculiar velocities for the ENEARc sample are reported in Section 4. In Section 5 we look for potential systematic effects which may invalidate the underlying assumption that galaxies in different clusters are similar. Finally, in Section 6 we present a brief summary of our results.

## 2. The Cluster Sample

The spectroscopic and photometric parameters for the 452 galaxies in 28 clusters used here are presented in B01, where we describe the selection of the cluster sample and membership assignments. The clusters we consider in the present study span the redshift range  $1000 \lesssim cz \lesssim 11,000 \text{ kms}^{-1}$ , covering both equatorial hemispheres. The characteristic parameters (mean redshift, size and velocity dispersion) of nearly all clusters were computed from the analysis of “groups” identified using objective friend-of-friends algorithms applied to complete redshift surveys (see B01). Exceptions include the Centaurus complex, three clusters previously studied by Jørgensen, Franx, & Kjærgaard (1995a, 1995b) and Jørgensen (1997) (A539, AS639, and A3381), and two observed by Smith et al. (1997) (7S21 and A347). The parameters adopted for these cases and the reasons for including them are discussed in B01. Using the identified groups as signposts for clusters, galaxies fainter than the ENEAR magnitude limit ( $m_B \sim 14.5$ ) were considered members by adopting well-defined position and kinematic criteria which should minimize errors in the membership assignment. About 2% of the galaxies previously assigned to clusters were found not to be members according to the membership criteria adopted.

The data set of the ENEARc sample is a compilation including new photometric and spectroscopic measurements obtained as part of this program as well as data previously reported in the literature. In B01 we presented the photometric and spectroscopic measurements for 640 individual cluster galaxies, including new measures of the photometric parameter  $d_n$  for 348 galaxies, new spectroscopic measurements of redshift, velocity dispersion and the  $\text{Mg}_2$  index for 229 galaxies. Our new data for cluster galaxies have been combined with those in the literature by converting all measurements to a common system (see B01). This was possible by securing observations for a representative number of galaxies in common with other samples, thus allowing the definition of conversion relations. Data from the literature come from Dressler (1987), Lucey & Carter (1988), Faber et al. (1989), Dressler, Faber, & Burstein (1991), Jørgensen et al. (1995a, 1995b), Lucey et al. (1997), and Smith et al. (1997). A detailed description of the new  $R$ -band imaging data and parameters, including the total magnitude, the effective radius  $r_e$ , mean surface brightness within this radius  $\mu_e$  and disk-to-bulge ratio  $D/B$  will be presented in Alonso et al. (2001) while the spectroscopic data will be presented by Wegner et al. (2001).

In constructing the  $D_n - \sigma$  relation, we exclude 188 galaxies (see B01, Table 8) either because they present photometric or spectroscopic features typical of later type galaxies (e.g., presence of arms, bar, dust lane, emission lines) or because the measured parameters could be affected due to contamination by nearby galaxies or stars. Pruning the sample in this way decreases the scatter ( $\sim 5\%$ ) but leaves both the slope and zero-point essentially unchanged.

The selection and completeness of the sample of early-type galaxies in clusters is not very well defined because: a) it varies from cluster to cluster; and b) each cluster is a compilation of galaxies taken from different sources. The sample of cluster galaxies includes: i) all early-type galaxies brighter than  $m_R < 14.5$  (since they were extracted from complete magnitude-limited catalogs, see da Costa et al. 2000a); ii) fainter early-types with photometric and spectroscopic data available in the literature (see B01). Furthermore, for any given  $S/N$  and resolution, there is a lower limit below which the velocity dispersion measurements are unreliable. Since a cluster may have measurements taken from different sources, this lower limit is not well defined either. For example, for some sources in the literature only measurements of  $\sigma > 100 \text{ kms}^{-1}$  are available; for our data this limit can be as low as  $45 \text{ kms}^{-1}$  due to the higher resolution used (see Wegner et al. 2002). We have checked that the results presented below are not significantly dependent on the adopted velocity dispersion limit.

### 3. Determining the distance relation

#### 3.1. The method

A galaxy’s angular size varies inversely as  $R$ , its co-moving distance. If  $d_n$  is the measured size of the galaxy on the sky, then  $1/d_n$  is a measure of its distance. The central velocity dispersion of a galaxy  $\sigma$  is expected to be correlated with its physical size  $D_n \equiv d_n \times R$  (e.g. Dressler et al. 1987). If we measure both  $d_n$  and  $\sigma$ , then the basic distance indicator becomes

$$\log R = a \log \sigma - \log d_n + b, \quad (1)$$

where  $a$  represents the scaling of velocity dispersion with size:  $D_n \propto \sigma^a$ . Here both  $R$  and  $\sigma$  are in units of  $\text{kms}^{-1}$ , and  $d_n$  is expressed in units of 0.1 arcmin. Define the quantities  $y \equiv \log D_n + \log h$ , where  $h = H_o/(100 \text{ kms}^{-1}\text{Mpc}^{-1})$ , and  $x \equiv \log \sigma$ . Then the distance relation is

$$y = ax + b. \quad (2)$$

The slope of equation (2) is usually determined using cluster galaxies, because they can be assumed to be equally distant and the uncertainty in the estimated distances falls as  $1/\sqrt{N}$ . If a distance relation which does not depend on cluster properties exists, it can be determined by combining the data from all available clusters to produce a standard template relation. Although the peculiar velocity field is unknown, combining many different clusters should improve the statistical accuracy of the slope and zero-point. (Note that here we are only assuming that early-type galaxies in different clusters are similar; we are not addressing the possible differences between galaxies in clusters and in regions of lower density.)

Here, the template parameters—zero-point, slope, and relative motions of each cluster—are determined simultaneously. Such a procedure has been adopted by a number of authors (Baggley 1996; Giovanelli et al. 1997, hereafter G97; Scodreggio 1997; Scodreggio et al. 1998; Colless et al. 2001) in determining the  $D_n - \sigma$ , FP and TF relations. Our notation below follows G97. The distance relation can be derived by either a direct (forward) or inverse linear regression fit, depending on whether the slope is obtained using the distance-dependent  $d_n$  or the distance-independent parameter  $\sigma$  as the independent variable. We study the direct first and the inverse later, in Section 3.3.

The coefficients of the direct relation  $y = a_d x + b_d$  are determined as follows. We have  $N_g$  galaxies in  $N_{cl}$  clusters. Let  $(x_{ik}, y_{ik})$  denote the values of  $x$  and  $y$  for the  $i$ -th galaxy in the  $k$ -th cluster. For the  $k$ -th

cluster, the distance relation is  $y = a_k x + b_k$ . Our assumption that the distance relation does not depend on the properties of a cluster means that  $a_k$  has the same value,  $a_d$ , for all clusters. If as a first guess one uses the observed radial velocity  $cz$  as the “distance” ( $y \equiv \log D_n + \log h \equiv \log(d_n \times cz) + \log h$ ), the zero-point  $b_k$  is different for different clusters only because of their peculiar velocities relative to the Hubble flow:  $b_k = b_d + \Delta_k$ . We would like to find those values of  $a_d$ ,  $b_d$  and  $\Delta_k$  for which the scatter around the mean relation is minimized. Therefore, we minimize

$$\chi^2 = \sum_{k=1}^{N_{cl}} \sum_{i=1}^{N_g(k)} \left[ \frac{y_{ik} - (a_d x_{ik} + b_d + \Delta_k)}{\sigma_{ik}} \right]^2, \quad (3)$$

with respect to the slope  $a_d$ , the zero-point  $b_d$ , and the relative offsets  $\Delta_k$ . Here  $\sigma_{ik}$  is related to the measurement error in  $D_n$  of the  $i$ -th galaxy in the  $k$ -th cluster.

If “distant” clusters (which we define as being clusters beyond  $3000 \text{ km s}^{-1}$ ) are at rest relative to the CMB then the sum over their peculiar velocities should equal zero. Therefore, once  $a_d$ ,  $b_d$  and the  $\Delta_k$ ’s have been found, we compute

$$\sum_k N_g(k) \Delta_k / \sum_k N_g(k)$$

where the sum is over the subset of “distant” clusters in our sample. We then subtract this value from each of the  $\Delta_k$ ’s. In effect, this sets the overall zero-point of the distance relation.

As will be shown below, this condition turns out to be equivalent to requiring (i) the distance to Virgo equal that given by the Cepheid period-luminosity relation (Kelson et al. 2000), or (ii) assuming that the Coma cluster is at rest.

Formally, the equations above fully describe the procedure we use to determine the parameters which describe the distance relation. However, when working with real data, one must also consider possible sources of bias (for a review, see Strauss & Willick 1995 and references therein), as described below.

### 3.2. Monte-Carlo Bias Correction

For the direct relation, i.e., when fitting on the distance-dependent parameter, the most pernicious bias is that due to incompleteness. This bias leads to a shallower slope, a larger zero-point, and an underestimate of the scatter. Although analytic bias-correction schemes have been proposed (Willick 1994), the assumptions made are hardly met by real data. This bias is particularly difficult to handle when the completeness varies from cluster to cluster, as is the case in our sample. Here we follow G97, Scodreggio (1997) and Scodreggio et al. (1998) and use a Monte-Carlo approach to estimate the bias correction, although this is not the only method that can be used (Wegner et al. 1996).

As mentioned above, to estimate the bias, we must first know the incompleteness in  $D_n$  for each cluster. This requires knowledge of the  $D_n$  distribution function, the counterpart of the luminosity function. Since this function is not directly available, two approaches are possible: (i) assume that a fair representation of this distribution is given by that of a nearby cluster which is complete; (ii) examine the correlation of  $d_n$  with some other measure of the angular size of a galaxy, whose distribution is known. We adopt the second approach.

Let  $\theta_{25}$  denote the angular diameter enclosing an integrated surface brightness of  $25 \text{ mag arcsec}^{-2}$ , and let  $D_{25}$  denote the physical size obtained by multiplying this angular size by the distance to the galaxy. The

distribution of  $D_{25}$  in the ESO-LV catalog (Lauberts & Valentijn 1989) is

$$\phi(D_{25}) dD_{25} \propto \exp\left(\frac{-D_{25}}{D_\star}\right) \frac{dD_{25}}{D_\star}, \quad (4)$$

with  $D_\star = 2610 \text{ kms}^{-1}$  (Sodré & Lahav 1993). There is a tight correlation between  $d_n$  and  $\theta_{25}$  (e.g., Wegner et al. 1996), so the distribution of  $D_n$  in a complete sample should be well approximated by

$$\Phi(D_n) = \phi(D_{25}) \frac{dD_{25}}{dD_n}. \quad (5)$$

The results are insensitive to the exact shape of the diameter function (e.g., G97). The ratio of the observed distribution of  $D_n$  in a given cluster with the one expected for a complete sample provides an estimate of the completeness. This ratio depends on  $D_n$  differently for each cluster: we call it the completeness  $C_k(D_n)$ . Note that  $C_k(D_n)$  varies between zero and one.

Incompleteness leads to a bias in determining the distance indicator coefficients  $a_d$  and  $b_d$ , which we estimate using the following Monte-Carlo approach. In the first step, distances to clusters are approximated by using their redshifts, and the  $\chi^2$  defined in equation (3) is minimized. This provides initial guesses for the slope, zero-point, peculiar velocities, and scatter  $\epsilon$  around the mean relation. The scatter  $\epsilon$  may change with velocity dispersion, so we actually compute  $\epsilon(x)$  in bins of  $x$ .

For the  $i$ -th galaxy in the  $k$ -th cluster a bias correction  $B_{ik}$  is obtained as follows. A Gaussian zero mean unit variance random number  $g$  is generated. This, with the coefficients  $a_d$  and  $b_d$  and the scatter  $\epsilon(x_{ik})$ , is used to compute  $y_{ik}^s = a_d x_{ik} + b_d + g\epsilon(x_{ik})$ . This represents the value of  $y$  the observed galaxy may have had. If this value of  $y$  was too small, the galaxy would not have been observed. The probability it would have been observed is proportional to the completeness  $C_k(y_{ik}^s)$ . Therefore, we generate a random number  $u$  which is distributed uniformly between zero and one. The number  $y_{ik}^s$  is accepted if  $u \leq C_k(y_{ik}^s)$ . We repeat this procedure until we have accepted 500 values of  $y_{ik}^s$  for each galaxy. The mean of these values  $\langle y_{ik}^s \rangle$  reflects the incompleteness of the real sample. It thus allows a direct estimate of the bias:

$$B_{ik} = \langle y_{ik}^s \rangle - (a_d x_{ik} + b_d). \quad (6)$$

This value is used to define corrected values

$$y_{ik}^c = (a_d x_{ik} + b_d) - B_{ik}. \quad (7)$$

These corrected values are inserted in equation (3); minimizing yields new estimates of  $a_d$ ,  $b_d$ , the  $\Delta_k$ s, and the scatter  $\epsilon$ . The process is repeated until convergence is reached; applied to our data, this happens after about four iterations.

### 3.3. The Template Distance Relation: Fitting Parameters

We apply the above procedure to the cluster sample presented in Section 2. We start by assuming that the clusters are at rest relative to the Hubble flow and that their distances are given by the mean cluster redshift (see B01). Figure 1 shows the individual uncorrected cluster data at the start of the iterative process. The solid line represents the best fit after minimizing  $\chi^2$  (equation 3) for the first time. Note that the number of galaxies in each cluster varies dramatically and, for most groups, only the more luminous, high velocity dispersion cluster galaxies are included in the sample. Therefore, if the selection bias correction

is not applied, a significant bias exists in the global template constructed using all clusters. The relative offsets between those data points and the distance relation reflect the relative motions of the clusters.

Figure 2 shows the completeness function  $C(D_n)$  for each cluster computed from the ratio between the number of objects observed in the cluster to the number predicted by the fitted diameter-distribution function (equation 5).

In practice, this is done after binning the data in  $\Delta y \equiv \Delta \log D_n = 0.2$  bins, and then smoothing with a Hanning filter (convolving with a [0.25, 0.50, 0.25] function) to reduce the effects of small number statistics. The solid curve is a fit to the histograms using the function (G97)

$$C(y) = \frac{1}{1 + e^{(y-y_f)/\eta}} \quad (8)$$

to represent the completeness function, thereby further reducing the effects of small number statistics. Table 1 gives the parameters  $y_f$  and  $\eta$  of the completeness function for each cluster. At the bright end (large values of  $y$ ) the completeness was normalized to unity, based on the fact that in all clusters the brightest galaxies are always included in the cluster sample. Comparison between the predicted and observed diameter-functions for the nearby Virgo cluster are in good agreement down to small values of  $D_n$ , indicating that we could have used Virgo to estimate the completeness of the other clusters.

Using this function as input, we estimated the bias correction  $B_{ik}$  for the  $i$ -th galaxy in the  $k$ -th cluster. The results after the final iteration are shown in Figure 3. For nearby clusters, such as Virgo and Fornax, the incompleteness bias correction is small, as expected. For more distant clusters the correction can be significant, with  $\Delta y \sim 0.1$  (corresponding to  $\Delta m \sim 0.5$  mag).

After the iterating, final values for the distance relation coefficients are determined. Applying the condition that “distant” clusters, i.e., clusters beyond 3000  $\text{kms}^{-1}$  (with a mean redshift of 6000  $\text{kms}^{-1}$ ), are at rest with respect to the CMB, and excluding clusters with suspiciously large peculiar velocities (see discussion below), we obtain the following final relation:

$$\log D_n = 1.203(\pm 0.023) \log \sigma_0 + 1.406(\pm 0.021), \quad (9)$$

where the error of the slope is derived by bootstrap re-sampling. The bootstrap error is based on the distribution of the slopes derived from a large number of data sets constructed through random sampling of the observed data set. The derived zero-point is consistent with the value obtained by using the distance of Virgo as determined by the Cepheid period-luminosity relation (Kelson et al. 2000). It is also consistent with the value obtained by assuming that Coma is at rest with respect to the CMB (the  $D_n - \sigma$  relation given above leads to a peculiar velocity of  $\sim -72 \pm 189 \text{ kms}^{-1}$  for Coma).

The error in the zero-point has two sources. The first is related to the scatter in the distance relation and the procedure adopted in the construction of the template relation. This was estimated as follows. We constructed data sets by randomly removing some points and replacing them with others from the observed data set. For each cluster the same fraction of data points were replaced, typically from 5% to 25%. For clusters with few members ( $\lesssim 10$ ) for which this was not possible due to the small number of cluster members, we left out one or two observations in sequence. We fixed the slope of the  $D_n - \sigma$  relation, and derived the zero-point from each simulated data set. The random uncertainty in the zero-point is given by the standard deviation of a Gaussian fit to the distribution of these zero-points. This yields an error of 0.018, corresponding to an error of  $\sim 4\%$  in distance. The second contribution to the zero-point error is the uncertainty in the mean velocity of the distant cluster sample used to set the zero-point of the relation. This

uncertainty is due to the finite number of clusters used to sample the peculiar velocity field of the clusters. It is also susceptible to cosmic variance. The uncertainty in the mean peculiar velocity of the cluster sample is given by  $\sigma/\sqrt{N}$ , where  $\sigma$  is the *rms* of the clusters’ peculiar velocity distribution and  $N$  is the number of clusters. Note, however, that since the clusters in our sample are not randomly distributed the actual number of clusters with uncorrelated velocities should be smaller than the 28 clusters considered. Here we estimate the error to be  $\sim 400/4 = 100 \text{ kms}^{-1}$ , which corresponds to  $100/4500 \sim 2\%$  at the median distance of the clusters in our sample. Adding in quadrature the different contributions to the error budget we estimate the final error in the zero-point to be 0.021, with the main contribution coming from the uncertainties associated with the distance relation.

Figure 4 shows the initial and final estimates of the distance relation together with the distribution of the observed *rms* scatter (solid histogram), and the intrinsic scatter (dashed histogram), as a function of  $\sigma$ . The intrinsic scatter was derived by subtracting the measurement uncertainties in quadrature from the *rms* scatter of the fit—although it increases at low  $\sigma$ , its mean value is  $\sim 0.06$  dex. This scatter may reflect differences in the stellar populations of the cluster member galaxies. This possibility will be discussed in Section 5.2. The intrinsic scatter limits the accuracy of the derived distances. The mean of the total scatter  $\bar{\epsilon} \sim 0.085$  dex, yields a distance error  $\Delta \sim 20\%$ . This is comparable to the errors obtained using FP relations (e.g., Hudson et al. 1997).

We used the Coma cluster to test if our correction based on Monte-Carlo simulations is reliable. For this cluster we extracted sub-samples using different magnitude-limits and computed the  $D_n - \sigma$  relation for each individual sub-sample as follows: a) without applying the bias correction described in Section 3.2, and b) correcting the slope for selection effects. We found that imposing a magnitude-limit biases the slope to lower values, but that the Monte-Carlo technique used recovers the correct value of the slope in each sub-sample. Using galaxies in Coma we also checked whether adopting different lower-limits in velocity dispersion biases the slope of the distance relation. We found that increasing the value of the velocity dispersion cutoff, for instance from 70 to 100  $\text{kms}^{-1}$  does not affect significantly our results, with the slope varying by less than 2% and the scatter remaining unchanged.

Figure 5 shows the bias-corrected data points for all clusters and the final fit. A number of interesting cases are evident. For instance, HMS0122+3305, A2199, Cen30, exhibit clear evidence of either spatial sub-structure or distinct galaxy populations, and the galaxies in the cluster AS714 do not strictly follow the template relation. The individual  $D_n - \sigma$  exhibit a tilt relative to the template relation. We will return to these points below.

To evaluate the robustness of our results, we derived the  $D_n - \sigma$  relation when specific sub-samples of galaxies were excluded. The results are summarized in Table 2: column (1) gives the sub-sample of galaxies removed (A = “peripheral” objects defined in B01; B = clusters whose individual  $D_n - \sigma$  relations differ significantly ( $\Delta \text{slope} \gtrsim 0.2$ ) from equation (9); and individual clusters); column (2) the number of remaining galaxies which were used to compute the  $D_n - \sigma$  relation; column (3), (4) and (5) the slope, the zero-point, and the *rms* scatter of the  $D_n - \sigma$  relation obtained using the number of galaxies given in column (2). Based on these tests we conclude that the variation of the slope,  $a$ , agrees with the formal error computed from the bootstrap re-sampling ( $\sigma_a \sim 0.023$ ).

We have also computed the direct relation using orthogonal fits, allowing for errors in both  $\log D_n$  and  $\log \sigma$ , and for the inverse relation, ignoring the bias correction. The results are shown in the upper and lower panels of Figure 6. The corresponding coefficients and scatter in  $\log D_n$  are given in Table 3. The inverse relation is insensitive to the photometric selection and is, in principle, bias-free if no a priori cut



is made in that variable (see Strauss & Willick 1995). However, as some data from the literature in our sample are limited to galaxies with  $\sigma \gtrsim 100 \text{ kms}^{-1}$ , this assumption may not hold and, perhaps, in these cases treatment similar to that carried out for the distance-dependent parameter should be considered.

The three fitting relations in Table 3 clearly show that it is crucial to use a self-consistent fitting algorithm, to have a large and homogeneous set of data, and to correct for selection biases. For this analysis we found that even though the slopes and zero-points of the direct, bivariate, and inverse relations differ by more than  $2\sigma$ , the distances of the 28 clusters in the ENEARc sample agree well (see Section 4 and Figure 11).

The coefficients determined from our sample are compared with those found by other authors in Table 4. Our results are generally in good agreement with previous determinations, except for those of Baggley (1996) and Lucey et al. (1997). Saglia et al. (2001) have recently revised Baggley’s result giving both a slope and zero-point comparable to our values. Lucey et al. used two distant clusters, A2199 and A2634, to obtain their results. Our analysis shows that A2199 has an individual  $D_n - \sigma$  relation which differs significantly from equation (9) (see Table 6), while A2634 has a high peculiar motion (see next section for more details).

#### 4. Cluster Peculiar Velocities

We compute distances to galaxies in clusters using the “direct” template relation found in the previous section. Figure 7 shows the differences in distance between each individual galaxy and its cluster, the distance of which was computed as the error-weighted mean of the galaxy distances in the cluster. For the best sampled clusters (e.g., Virgo, Fornax) the distance distributions have well defined peaks and small scatter, resulting in good mean distances. However, there are a few complex cases where clusters exhibit sub-structure (e.g., HMS0122+3305, Perseus, Coma, and Cen30). Also, there are clusters which either show large scatter and poorly defined peaks (e.g., A2199, A2634, and Klemola44). And finally, there are clusters which have only a few galaxies; typically, these are either nearby small groups (e.g., 7S21, A347, A1367, HG50, Pegasus, Doradus, AS714) or very distant clusters (e.g., A3381) with large distance uncertainties.

The cluster distances were corrected for homogeneous Malmquist bias (following Lynden-Bell et al. 1988, the estimated distance is multiplied by  $\exp(3.5\bar{\epsilon}^2/N_g)$ , where  $N_g$  is the number of cluster galaxies); this correction generally amounts to less than  $\sim 3\%$  of the distance for the smallest groups.

The radial component of the peculiar velocity of each cluster,  $v_p = cz_{\text{cor}} - R$ , was computed using the Malmquist corrected distance  $R$ , and the mean cluster radial velocity  $cz$  presented in B01 and corrected for the cosmological effect:

$$cz_{\text{cor}} = cz - \log \left( \frac{1 + (7/4)(cz/c)}{1 + (7/4)(cz_{\text{Coma}}/c)} \right) \quad (10)$$

where  $cz_{\text{Coma}}$  is the Coma cluster radial velocity and  $c$  is the speed of light (Lynden-Bell et al. 1988). Baggley (1996) computed a more accurate cosmological correction, but for nearby galaxies equation (10) is a good approximation.

The measured cluster distances and peculiar velocities are presented in Table 5: column (1) gives the cluster name; column (2) the number of observed cluster galaxies; columns (3) and (4) are the cluster’s Galactic coordinates; column (5) its redshift determined from the group finding algorithm (see B01) and its error in the CMB frame; column (6) is the computed cluster distance and its error; and column (7) gives the cluster peculiar velocity and its error in the CMB frame.

How the sample of galaxies in a cluster is chosen can lead to significant differences in the determined mean velocity. Figure 8 shows the galaxy redshift distribution in each cluster. Open histograms show the distribution of differences in redshift between the individual galaxies and the redshift assigned to the cluster. Solid histograms show this distribution for galaxies which were selected by applying the group-finding algorithm to complete but magnitude-limited redshift surveys (see Section 2). The figure shows that the fraction of galaxies in some clusters identified by the algorithm is significantly smaller than the total number of galaxies used in this paper (e.g., Coma). For such clusters, using all galaxies (open histograms) or using only this subset (filled histograms) may provide different estimates of the cluster’s mean redshift, velocity dispersion, and other parameters. Nevertheless, the figure suggests that the mean redshift remains about the same, even though the solid histograms are likely to underestimate the dispersion around the mean redshift.

The error-weighted mean cluster redshift of early-type galaxies only (long vertical line) and that given by the group finding algorithm (short vertical line) are also shown in Figure 8. For the latter, the sample of galaxies assigned to a group/cluster included all morphological types. Note the significant redshift differences, occasionally as large as  $300 \text{ km s}^{-1}$ . The most deviant cases ( $\gtrsim 2\sigma$ , where  $\sigma$  is the error in the mean cluster redshift of early-type galaxies – i.e., the error on the position of the long vertical line) are A347, A539, A1367, Eridanus, Doradus, and Pavo II. This suggests that using a sub-sample of galaxies in a cluster (especially when only few objects are selected) to compute the cluster redshift may introduce an error which can, in some cases, be large. This possibility has been ignored in the past, and may account for some disparities in the measurements of the peculiar velocity.

The upper panel of Figure 9 shows the distribution of cluster peculiar velocities. The lower panel shows that velocities do not depend on the estimated distances; large peculiar velocities occur both at small and large distances. Filled symbols are for the “distant” clusters used in the final calibration of the  $D_n - \sigma$  relation—the subsample which is required to be at rest relative to the CMB. Open circles indicate nearby clusters plus three additional clusters in the Great Attractor (e.g., Lynden-Bell et al. 1988) region: Cen30, AS714, and AS753. Triangles show clusters with data exclusively from the literature. The  $1\sigma$  error bars were computed by adding the distance and the cluster mean redshift errors in quadrature. The errors in distances were taken to be  $\Delta/\sqrt{N}$ , where  $\Delta$  is the fractional distance error derived from the scatter of the composite distance relation, and  $N$  is the number of galaxies observed in the cluster. The error in the cluster redshift is estimated as  $\sigma_{cl}/\sqrt{N'}$ , where  $\sigma_{cl}$  is the velocity dispersion of the cluster and  $N'$  is the number of galaxies in the group catalog.

The distribution shown in the upper panel of Figure 9, which includes all 28 clusters, has an error-weighted mean of  $151 \pm 75 \text{ km s}^{-1}$ , with a scatter of  $399 \pm 73 \text{ km s}^{-1}$ . The bottom panel shows that there are three obvious outliers: A2634, AS639, and Cen45, all based on data from the literature. Other clusters with large ( $> 2\sigma$ ) peculiar velocities are Cen30 ( $500 \pm 153 \text{ km s}^{-1}$ ), AS714 ( $559 \pm 245 \text{ km s}^{-1}$ ), and AS753 ( $812 \pm 204 \text{ km s}^{-1}$ ); all are located near the Great Attractor. If these clusters are removed from the sample, the mean peculiar velocity of the remaining 22 clusters is  $71 \pm 51$  and the *rms* one-dimensional cluster velocity is  $239 \pm 46 \text{ km s}^{-1}$ . This is comparable to what is measured from the SCI sample (G97)  $266 \pm 30 \text{ km s}^{-1}$  (Giovanelli 1998). This small one-dimensional *rms* cluster velocity has important implications for cosmological parameters (e.g., Giovanelli 1998; Borgani et al. 2000a).

Notes to additional problematical clusters can be found in Appendix A. Most of these clusters appear to suffer from the effects of substructure; they have a history of discrepant peculiar motions reported in the literature.

The large overlap between our cluster sample and the literature allows a global comparison of the measured peculiar velocities. Figure 10 shows our cluster peculiar velocities ( $v_p$ ), computed using the direct  $D_n - \sigma$  relation, for the clusters we have in common with Jørgensen et al. (1996) (10 clusters), SCI (11 clusters), Hudson et al. (1997) (15 clusters), and Gibbons et al. (2001) (15 clusters). This figure shows that except for A2634, A194, and AS753 our measurements of the cluster peculiar velocities are in good agreement with those reported in literature when the measurement errors are taken into account. We find mean differences of  $79 \pm 91 \text{ kms}^{-1}$  (Jørgensen et al.),  $182 \pm 94 \text{ kms}^{-1}$  (SCI),  $-9 \pm 96 \text{ kms}^{-1}$  (Hudson et al.) and  $-53 \pm 93 \text{ kms}^{-1}$  (Gibbons et al.). All clusters are in the same rest frame to within  $2\sigma$ . This agreement shows consistency between different determinations of cluster distances (e.g., those based on the  $D_n - \sigma$  and/or FP relation) and, more importantly, consistency with the TF relation for spiral galaxies.

Figure 11 compares the peculiar velocities computed using the bivariate relation, corrected for selection bias (left panel), and the inverse relation (right panel) with those determined using the direct relation. The mean differences are  $-43 \pm 32 \text{ kms}^{-1}$  with a scatter of  $74 \text{ kms}^{-1}$ , and  $-58 \pm 38 \text{ kms}^{-1}$  with a scatter of  $89 \text{ kms}^{-1}$  for the bivariate and inverse relations, respectively. This shows that the peculiar velocities of the clusters are largely insensitive to the fitting procedure, whether the direct, bivariate or inverse relation is used.

## 5. Dependence of the distance relation on galaxy properties

To use the composite  $D_n - \sigma$  relation as a distance indicator, we should demonstrate that systematic cluster-to-cluster differences are small and that the computed cluster distances are unaffected by differences in the morphological mix of the galaxy population, different stellar populations or other cluster properties. Furthermore, the measured peculiar velocities must be free of any other systematic effects such as extinction, and contamination by interlopers. This can be tested by examining the residuals from the distance relation which, for our data, exceed the estimated measurement errors of the  $D_n - \sigma$  parameters. (Note that testing to see if the distance relation depends on whether or not the galaxies are in clusters or in less dense environments is not the subject of this paper.) All the tests below suggest that cluster-to-cluster variations are indeed small.

### 5.1. Results for individual clusters

Figure 12 plots the measured values of  $D_n$  and  $\sigma$  for the galaxies in each cluster along with the (incompleteness corrected) fit (dashed line) and the composite template relation (solid line). The parameters for the individual fits are given in Table 6: column (1) gives the cluster name; column (2) the number of cluster galaxies entering the  $D_n - \sigma$  relation; column (3) the slope and its error; column (4) the mean scatter in  $\log D_n$  of the data points relative to the individual fit; column (5) the zero-point offset between the individual and the composite template relation (equation (9)); column (6) the scatter relative to the fit obtained using the slope of the composite template relation but allowing the individual zero-point to vary; column (7) the intrinsic scatter computed using the scatter listed in column (6) and the errors of the measured parameters; and column (8) gives the fraction of the cluster galaxies in the observed sample that are ellipticals ( $F_E = N_E / (N_E + N_{S0})$ ).

Figure 12 shows that for most clusters the individual fits have nearly the same slope as the template. The figure also shows the benefit of combining all the data, because the slope for the poorer systems in the sample

is poorly determined. Significant departures ( $\Delta$  slope  $\gtrsim 0.2$ ) are seen for HMS0122+3305, A1367, HG50, A2199, Doradus, A3381, AS639, Cen30, and AS714. The main cause for the tilt of an individual  $D_n - \sigma$  is the small number of galaxies in the cluster. (For example, Table 6 shows that the tilt of the individual  $D_n - \sigma$  relations does not correlate with the fraction of ellipticals in the cluster, although some incorrect morphological classifications may still be present.) Indeed, even a single galaxy can cause a significant deviation from equation (9). As discussed above (see also Appendix A), many of these clusters show large motions. Also, recall that A2199 and Cen30 are parts of two-component systems (A2199-97 and Cen30-45).

In general, Table 6 shows that the individual fit does not improve the scatter significantly and that variations are likely due to poor statistics. The source of the intrinsic scatter is still not understood, though the largest contributions to it probably arise from intrinsic differences in the dynamical structures of the cluster galaxies rather than from errors in the photometry and spectroscopy. Whether these intrinsic differences produce systematic errors in the distance determination is unknown. However, because we treat the thickness of the relation as an uncertainty in the derived distance, the impact of such scatter should not alter our conclusions about large-scale motions in the universe (see also Section 5.2).

Figure 13 can be used to examine the impact of interlopers. It shows the residual of each galaxy from the distance relation as a function of the difference between the galaxy’s redshift and that of the parent cluster. Field galaxies contaminating the sample would lie along the  $45^\circ$  line shown in each panel—no such effect is seen. This is a consequence of our membership assignment and the fact that early-types are more likely to reside at the central regions of clusters.

To study the effects of morphology, we split the sample into ellipticals ( $T \leq -3$ ) and S0s ( $T = -2$ ), using Lauberts & Valentijn’s (1989) classifications. First, we computed the  $D_n - \sigma$  relation for the E and S0 galaxies separately. Figure 14 shows these relations for the ellipticals (left panel) and S0s (right panel); the difference in the slope of the two distance relations is  $0.071 \pm 0.059$ , which is significant at  $< 2\sigma$  level, and the scatter is comparable. Second, we determined the relative shifts which were required if a linear relation of the same slope as of the composite template relation ( $a = 1.203$ , see Equation 9), was to fit the relation in each of the subsamples. The difference in the intercept is not statistically significant and the scatter is comparable. These results justify our neglect of any morphological biases (Section 3.1).

To test further the above result one could, instead, consider the residuals in the  $D_n - \sigma$  relation as a function of the  $D/B$  ratio. Unfortunately, in practice,  $D/B$  is available only for those galaxies in our sample which were observed by us; the data compiled from the literature used one component models to derive global photometric parameters. The 223 cluster galaxies for which we have our own photometric measurements show no correlation between the residuals of the  $D_n - \sigma$  relation and the  $D/B$  ratio (see Figure 15).

## 5.2. Stellar Populations

Earlier in this paper we found that the scatter of galaxies relative to the template distance relation is roughly twice what can be accounted for by measurement errors. The additional scatter has been attributed, by several authors, to differences in stellar populations. In the context of distance measurements, we must check if these differences can lead to systematic errors in the distance, and therefore to spurious peculiar velocities.

To study the effects of different stellar populations, we use the  $Mg_2 - \sigma$  relation, which is supposed to be distance independent. It was computed for all galaxies in the sample after sorting them according to

their morphological types (see Figure 16). The parameters of the orthogonal fits to the  $Mg_2 - \sigma$  relation are given in Table 7. Column (1) of the table gives the morphological types which are in the sample; column (2) the number of galaxies; column (3) the slope computed from the whole sample and its error; column (4) the zero-point and its error computed by fixing the slope to the value reported in column (3); and column (5) the scatter relative to the relation. Note that the coefficients describing the linear fit obtained here differ slightly ( $< 1\sigma$ ) from those of Bernardi et al. (1998). This is because we now include  $Mg_2$  measurements from other authors, scaling them to our system. The table shows small differences in the zero-point between ellipticals and S0s, although the S0 galaxies have a larger scatter than ellipticals. This is partially due to the small number of galaxies with low velocity dispersions in both sub-samples. Although one expects S0 galaxies to form a less uniform class of objects than ellipticals, the differences we find are small. Therefore, this analysis suggests that the  $D_n - \sigma$  relation does not depend on differences in stellar populations.

If differences in stellar populations were important in estimating distances, one would expect correlations between the  $D_n - \sigma$  and  $Mg_2 - \sigma$  residuals,  $\Delta(D_n - \sigma)$  and  $\Delta Mg_2$ , respectively, since the latter should reflect either age or metallicity differences. The left panels of Figure 17 show  $\Delta(D_n - \sigma)$  versus  $\Delta Mg_2$  for the cluster galaxies as a whole (upper panel); for the ellipticals (middle panel); and for S0s (lower panel), while the right panels show  $\Delta(D_n - \sigma)$  as a function of the  $Mg_2$  line index. As can be seen, there is no obvious correlation between these parameters. Applying the Spearman rank test to the data shown in the various panels, we find that the rank-order correlation coefficients vary from 0.10 to  $-0.15$ , implying significance levels  $> 0.8$ , thereby confirming the lack of any significant correlation between these quantities. These results are in agreement with the conclusions of previous studies (e.g., Jørgensen et al. 1996; Colless et al. 1999).

Figure 18 shows the data points for each cluster and the composite  $Mg_2 - \sigma$  relation (solid line) given by the sample as a whole. Open circles indicate S0 galaxies, and filled circles, ellipticals. From these panels, it is evident that S0 galaxies depart more from the composite relation than ellipticals, especially at smaller velocity dispersions. Nevertheless, most galaxies do lie along the globally derived relation. There are some exceptions which were observed by other authors; these are listed in Appendix B.

Our results suggest that differences in stellar populations do not influence the distance relation enough to mimic peculiar motions. Furthermore, none of the most discrepant peculiar velocities discussed in the previous section show evidence that their velocities are caused by stellar population effects.

### 5.3. Environment

In the literature, there is concern that there may be cluster-to-cluster environmental differences in the  $D_n - \sigma$  method and here we examine this possibility. Figure 19 shows the distribution of the intrinsic scatter ( $\bar{\epsilon}_{intr}$ ) and the slope of the fit as a function of: a) the measured velocity dispersion of the cluster  $\sigma_{cl}$ ; and b) the logarithm of the ratio  $\sigma_{cl}^2/R_p$ , where  $R_p$  is the pair radius defined by Ramella, Geller, & Huchra (1989) and  $\sigma_{cl}^2/R_p$  is a rough measure of the projected cluster surface density. Clusters/groups with poorly defined slopes (those with an error in the slope  $\gtrsim 0.1$ ; see Table 6 and Figure 12) are shown as crosses. Also represented by crosses are the points corresponding to the systems HMS0122+3305, A2199 and Cen30, where possible membership assignment problems may affect the determination of the slope (see B01). Seven clusters from the literature, for which values for  $R_p$  are not available, have not been included in the right panels of the figure (see B01).

Applying the Spearman rank test the whole sample confirms that there is no obvious correlation between the intrinsic scatter and the parameters that characterize the global properties of the clusters. The rank-

order correlation coefficients are 0.01 and  $-0.05$  with significance levels of 0.96 and 0.77, respectively. On the other hand, a similar analysis of the data shown in the bottom panels of Figure 19 might lead one to suspect that the slope of  $D_n - \sigma$  relation depends both on the velocity dispersion and on the surface density. Taking all the available data points into consideration the Spearman rank test gives a rank-order correlation coefficient of  $\sim 0.60$  with significance levels of  $\sim 5 \times 10^{-4}$  in both cases, indicating a strong correlation between the slope and  $\sigma_{cl}$  or  $\log \sigma_{cl}^2/R_p$ . However, the slope of individual cluster/group relations is in many cases poorly determined either because of the small number of measured cluster members or because of interlopers. In fact, if systems with large errors in the slope (nine systems) and cases where the slope could be affected by the presence of interlopers (three systems) are discarded, the Spearman rank-order correlation coefficient decreases to  $\sim 0.40$  corresponding to a significance level of  $\sim 0.15$  for both relations; this shows that the correlation between the slope of the  $D_n - \sigma$  relation and the velocity dispersion or central surface density is not significant. Clearly, a more definite test of this hypothesis requires considerable more data per cluster than currently available. We should also point out that the Spearman rank test also shows that there is no obvious correlation between either the intrinsic scatter or the slope of the cluster’s individual  $D_n - \sigma$  relation and the number of observed galaxies. The derived rank-order correlation coefficients are 0.32 and 0.11, yielding significance levels of 0.4 and 0.8, respectively. It should be emphasized at this point that the good agreement in the peculiar velocity field obtained from spirals and ellipticals give further support to the hypothesis of a universal distance-relation.

Gibbons et al. (2001) used 20 clusters, of which 15 are in common with us, to argue that the amplitude of the measured peculiar velocity correlates with the scatter of the distance relation. The left panel in Figure 20 shows the cluster peculiar velocities of all the clusters in our sample as a function of the amplitude,  $\bar{\epsilon}_{intr}$ , of the intrinsic scatter of the individual  $D_n - \sigma$  relations. The panel on the right shows the fraction of elliptical to early-type galaxies ( $N_E/(N_E + N_{S0})$ ) (right panel), versus  $\bar{\epsilon}_{intr}$ . These plots are similar to those shown by Gibbons et al. (2001). However, in contrast, we find no significant correlations in either relation. The Spearman rank test gives a rank-order correlation coefficient of 0.21 with a significance level of 0.28 for the  $v_p - \bar{\epsilon}_{intr}$  relation, and correlation coefficient of  $-0.16$  with a significance level of 0.40 for the relation shown in right panel.

We conclude that cases of poor fits are more likely to be due to observational limitations rather than reflecting intrinsically different physical properties. In summary, we find no compelling evidence that the peculiar velocities are spurious artifacts. Rather, we believe our quoted velocities do measure the motion of clusters relative to the Hubble flow.

## 6. Summary

Using new and previously published data for 452 galaxies in 28 clusters we have derived a bias-corrected  $D_n - \sigma$  relation. It can be used to measure relative distances of galaxies in the recently completed survey of early-type galaxies (da Costa et al. 2000a) and to map the peculiar velocity field. Our main conclusion are:

1. The slope obtained by combining data for all cluster/groups does not differ significantly from previous determinations.
2. The scatter is found to be  $\sim 0.085$  dex implying a distance error of about 20% per galaxy, comparable to the error of FP relations. Note that  $D_n$  is, in general, less sensitive to seeing and easier to compute (e.g., fits to light profiles are not required).

3. Our cluster peculiar velocities are in good agreement with other determinations, in particular, with those based on spiral TF distances, further supporting the validity of the distance indicators.
4. As in previous work we find no evidence for systematic effects playing a role in the computed peculiar velocities. We believe that the peculiar velocities we present here are not artifacts but rather a true measure of the clusters' motions relative to the Hubble flow.
5. Of the 28 clusters in the sample, six show suspiciously large peculiar velocities (both infall and outflow). Five of these are likely due to small-scale dynamical effects, or contamination by other components. The remaining one is at low galactic latitude and may suffer from absorption effects. Eliminating these clusters we find that the cluster one-dimensional *rms* velocity is relative small  $239 \pm 46 \text{ kms}^{-1}$ , suggesting a fairly quiescent velocity field, consistent with the estimate obtained from the TF data.

The distance relations derived here have been used in previous papers of this series (da Costa et al. 2000b; Borgani et al. 2000b; Nusser et al. 2001; Zaroubi et al. 2001) to analyze the peculiar velocity field traced by early-type galaxies. This sample of early-types, comparable in size to the SFI sample of field spirals (Haynes et al. 1999a, 1999b), allows an independent analysis of the characteristics of the local velocity field, because it uses a different distance relation, and test particles which probe a different set of density regimes. The good agreement between our early-type cluster sample and the SCI spiral sample suggests that it should be possible to merge the ENEAR and SFI redshift surveys. This will provide the largest and most homogeneous all-sky sample of nearby galaxies available for cosmic flow studies, and will allow the universality of the results presented here to be checked directly.

The authors would like to thank the referee for all the helpful comments and all of those who have contributed directly or indirectly to this long-term project. Our special thanks to Otávio Chaves for his many contributions over the years. We would also like to thank D. Burstein, M. Davis, A. Milone, M. Ramella, R. Saglia, and B. Santiago for useful discussions and input. MB thanks the Sternwarte München, the Technische Universität München, ESO Studentship program, and MPA Garching for their financial support during different phases of this research. MVA thanks CNPq for different fellowships at the beginning of the project and the CfA and ESO's visitor programs for support of visits. MVA is partially supported by CONICET and SecyT. LNdC would like to extend his special thanks to David W. Latham who played a pivotal role at the early stages of this project. GW is grateful to the Alexander von Humboldt-Stiftung for making possible a year's stay at the Ruhr-Universität in Bochum, and to ESO for support for visits to Garching. Financial support for this work has been given through FAPERJ (CNAW, MAGM, PSSP), CNPq grants 201036/90.8, 301364/86-9 (CNAW), 301366/86-1 (MAGM); NSF AST 9529098 (CNAW); ESO Visitor grant (CNAW). PSP and MAGM thank CLAF for financial support and CNPq fellowships. Most of the observations carried out at ESO's 1.52m telescope at La Silla were conducted under the auspices of the bi-lateral time-sharing agreement between ESO and MCT/Observatório Nacional.

#### A. Notes on the most peculiar cluster velocities

A2634: one of the most distant clusters in the ENEARc sample ( $cz \sim 9000 \text{ kms}^{-1}$ ), has a large peculiar velocity (it is  $> 2\sigma$  from the mean defined by our full sample). We have no measurements of our own for the this cluster. Lucey et al. (1997) re-observed some of its galaxies and concluded that the original values of the central velocity dispersion were underestimated. This partially accounts for its large infall velocity. Here the

peculiar velocity was determined using the Lucey et al. (1997) estimates, converted to our system. Although our ( $\sim -1787 \text{ kms}^{-1}$ ) is smaller than the number reported in Faber et al. (1989) and Lucey et al. (1991) ( $-3400 \pm 600 \text{ kms}^{-1}$ ), it also disagrees with the more recent estimate from Lucey et al. (1997), and with estimate from the SCI sample of cluster spirals (G97). The Lucey et al. (1997) value is significantly smaller ( $\lesssim -700 \text{ kms}^{-1}$ ) than ours, with the actual value depending on the distance relation used (FP or  $D_n - \sigma$ ). In the SCI sample this cluster is nearly at rest relative to the Hubble flow. Hudson et al. (1997), using a sub-sample of the Lucey et al. (1997) data set and the FP relation in their paper, also find a small infall. However, using the slope of their  $D_n - \sigma$  relation, and a zero-point derived from the peculiar velocities of the other two clusters we have in common with them, A347 and 7S21 (because the zero-point of the  $D_n - \sigma$  relation is not reported in that paper), yields a peculiar velocity of  $-1582 \pm 635 \text{ kms}^{-1}$  for A2634, comparable to our value. We also note that A2634 has a nearby companion (A2166) at approximately the same redshift, which may affect membership assignment, and may explain the large variations in its measured peculiar velocity.

A3381: the most distant cluster/group in the ENEARc sample ( $cz_{cmb} = 11472 \pm 65 \text{ kms}^{-1}$ ) with only 6 early-type galaxies. This cluster was originally studied by Jørgensen et al. (1996) who reported a peculiar velocity of  $667 \pm 698 \text{ kms}^{-1}$ .

AS639: at low galactic latitude ( $b \sim 10^\circ$ ), was originally studied by Jørgensen et al. (1996) who found it outflowing at  $1295 \pm 359 \text{ kms}^{-1}$ . Correcting to our standard system, we find an amplitude of  $1615 \pm 433 \text{ kms}^{-1}$ . This may reflect differences in the galaxy sample, since we have removed ESO 264G024, 1037-4605, ESO 264IG030 NED03, and ESO 264IG030 NED02 from it (see Table 8 in B01). It may also reflect differences in the adopted distance relations. Jørgensen et al. argued that this large amplitude was partially due to stellar population differences (section 5.2). Using the correlation between the  $\text{Mg}_2$  line index and the central velocity dispersion, they argued that the amplitude of the motion was smaller than  $\sim 879 \pm 392 \text{ kms}^{-1}$ . Recently, Jørgensen & Jønch-Sørensen (1998), using additional data, find a peculiar velocity of  $838 \pm 350 \text{ kms}^{-1}$ . They argue that this is also an overestimate, because of evidence for an apparently younger stellar population. This cluster lies so close to the galactic plane that uncertainties in absorption correction may be large; these may lead to artificially high values of the peculiar velocity.

Cen 30 and Cen 45: their large peculiar velocities can be partially explained by the fact that they lie along the same line-of-sight and are part of a complex structure. In Figure 7, Cen30 shows a bi-modal distance distribution because it is difficult to assign galaxies to the different clumps. While clearly seen in the distance distribution, the bimodality is not evident in the redshift distribution in Figure 8. The large positive peculiar velocity of Cen45 is likely caused by its infall towards the more massive component of the system (e.g., Lucey & Carter 1988). Given the complexity of the Centaurus system one should be cautious when using Cen30 and Cen45.

AS714: suspiciously large amplitude, has 19 members, close to the minimum number required to be included in the cluster sample. We targeted all 8 early-types in it, of which six are lenticulars. One of these was excluded from the cluster sample used to derive the  $D_n - \sigma$  relation because it appears to be spiral (see B01, Table 8). The measured peculiar velocity,  $559 \pm 245 \text{ kms}^{-1}$ , is high. However, the group is located in the direction of the GA, which may account for the large amplitude (as for Cen30). Because of the complexity of the region, the large peculiar velocity can also arise from small-scale dynamical effects, such as those in Cen45.

AS753: also in the GA region, shows a large positive peculiar velocity of  $812 \pm 204$ , which is significantly larger than the  $279 \pm 182 \text{ kms}^{-1}$  obtained by Jørgensen et al. (1996). The difference between Jørgensen et al.



and us is partially due to the choices of the galaxy sample, the distance relation and our weighting procedures, illustrating how systematic rather than random errors can sometimes be responsible for significant differences in the measured peculiar velocity of individual clusters.

### B. Notes on the $Mg_2 - \sigma$ relation

The following galaxies lie off the  $Mg_2 - \sigma$  relation shown in Figure 18.

Perseus: PGC 012423 (Smith et al. 1997) shows a higher  $Mg_2$  index than that expected from the  $Mg_2 - \sigma$  relation.

A539: three galaxies (CGCG 421-015, CGCG 421-017, and 0514+0619a from Jørgensen et al. 1995b) show a lower  $Mg_2$  index. They are faint galaxies in a crowded background.

A3381: PGC 018554 (Jørgensen et al. 1995b) has a lower  $Mg_2$  line index than the expected one. The spectrum of this galaxy may be affected by the light of a nearby bright star.

Hydra: PGC 031765 (the only galaxy observed by us) also has a low  $Mg_2$  index. The spectrum of this galaxy indicates the presence of weak emission lines and, as pointed out by Jørgensen et al. (1995a), its image shows the presence of a weak shell.

AS639: all galaxies in this cluster, which is located at low galactic latitude, seem to lie below the relation (see Jørgensen et al. 1996; Jørgensen & Jønch-Sørensen 1998; see also Section 4). All data points for this cluster are from Jørgensen et al. (1995b).

## REFERENCES

- Alonso, M. V., Bernardi, M., Wegner, G. et al. 2001, in preparation
- Baggley, G. 1996, PhD Thesis, Oxford University
- Baugh, C.M., Cole, S., & Frenk, C.S. 1996, MNRAS, 283, 1361
- Bernardi, M., Renzini, A., da Costa, L. N., Wegner, G., Alonso, M. V., Pellegrini, P. S., Rit e, C. & Willmer, C. N. A. 1998, ApJL, 508, 143
- Bernardi, M., Alonso, M. V., da Costa, L. N., et al. 2001, submitted
- Borgani, S., da Costa, L. N., Zehavi, I., Giovanelli, R., Haynes, M. P., Freudling, W., Wegner, G. & Salzer, J. J. 2000a, AJ, 119, 102
- Borgani, S., Bernardi, M., da Costa, L. N., Wegner, G., Alonso, M. V., Willmer, C. N. A., Pellegrini, P. S., & Maia, M. A. G. 2000b, ApJL, 537, 1
- Bressan, A., Chiosi, C., & Fagotto, F. 1994, ApJS, 94, 63
- Colless, M., Burstein, D., Davies, R. L., McMahan, R. K. Jr., Saglia, R. P., & Wegner, G. 1999, MNRAS, 303, 813
- Colless, M., Saglia, R. P., Burstein, D., Davies, R. L., McMahan, R. K. Jr., & Wegner, G. 2001, MNRAS, 321, 277
- da Costa, L. N., Bernardi, M., Alonso, M. V., Wegner, G., Willmer, C. N. A., Pellegrini, P. S., Rit e, C., & Maia, M. A. G. 2000a, AJ, 120, 95
- da Costa, L. N., Bernardi, M., Alonso, M. V., Wegner, G., Willmer, C. N. A., Pellegrini, P. S., Maia, M. A. G., & Zaroubi, S. 2000b, ApJL, 537, 81
- Djorgovski, S. & Davis, M. 1987, Ap. J., 313, 59
- D’Onofrio, M., Capaccioli, M., Zaggia, S. R. & Caon, N. 1997, MNRAS, 289, 847
- Dressler, A. 1987, ApJ, 317, 1
- Dressler, A., Lynden-Bell, D., Burstein, D., Davies, R. L., Faber, S. M., Terlevich, R. J. & Wegner, G. 1987, ApJ, 313, 42
- Dressler, A., Faber, S. M. & Burstein, D. 1991, ApJ, 368, 54
- Faber, S. M., Wegner, G., Burstein, D., Davies, R. L., Dressler, A., Lynden-Bell, D., & Terlevich, R. J. 1989, ApJS, 69, 763
- Franx, M., Kelson, D., van Dokkum, P., Illingworth, G. & Fabricant, D. 1997, in Galaxy Scaling Relations: Origins, Evolution and Applications, ed. L. da Costa & A. Renzini (Berlin: Springer), p. 185
- Gibbons, R. A., Fruchter, A. S. & Bothun, G. D. 2001, AJ, 121, 649
- Giovanelli, R., Haynes, M. P., Herter, T., Vogt, N.P., da Costa, L.N., Freudling, W., Salzer, J.J. and Wegner, G. 1997, AJ, 113, 53 (G97)

- Giovanelli, R. 1998, *Wide Field Surveys in Cosmology*, 14th IAP meeting (Paris: Editions Frontieres), p. 109
- Haynes, M.P., Giovanelli, R., Salzer, J. J., Wegner, G., Freudling, W., da Costa, L. N., Herter, T. & Vogt, N. P. 1999a, *AJ*, 117, 1668
- Haynes, M.P., Giovanelli, R., Chamaraux, P., da Costa, L. N., Freudling, W., Salzer, J. J. & Wegner, G. 1999b, *AJ*, 117, 2039
- Hudson, M.J., Lucey, J. R., Smith, R. J. & Steel, J. 1997, *MNRAS*, 291, 488
- Jørgensen, I., Franx, M., & Kjørgaard, P. 1993, *ApJ*, 411, 34
- Jørgensen, I., Franx, M. & Kjørgaard, P. 1995a, *MNRAS*, 273, 1097
- Jørgensen, I., Franx, M. & Kjørgaard, P. 1995b, *MNRAS*, 276, 1341
- Jørgensen, I., Franx, M., & Kjørgaard, P. 1996, *MNRAS*, 280, 167
- Jørgensen, I. 1997, *MNRAS*, 288, 161
- Jørgensen, I. & Jønch-Sørensen, H. 1998, *MNRAS*, 297, 968
- Kelson, D. D., Illingworth, G. D., Tonry, J. L., Freedman, W. L., Kennicutt, R. J., Mould, J. R., Graham, J. A., Huchra, J. P., Macri, L. M., Madore, B. F., Ferrarese, L., Gibson, B. K., Sakai, S., Stetson, P. B., Ajhar, E. A., Blakeslee, J. P., Dressler, A., Ford, H. C., Hughes, S. M. G., Sebo, K. M., & Silbermann, N. 2000, *ApJ*, 529, 768
- Lauberts, A., Valentijn, E. A. 1989, in *The Surface Photometry Catalogue of the ESO-Uppsala Galaxies* (Garching: ESO)
- Lynden-Bell, D., Faber, S. M., Burstein, D., Davies, R. L., Dressler, A., Terlevich, R. J., & Wegner, G. 1988, *ApJ* 326, 19
- Lucey, J. R. & Carter, D. 1988, *MNRAS* 235, 1177
- Lucey, J. R., Gray, P. M., Carter, D. & Terlevich, R. J. 1991, *MNRAS*, 248, 804
- Lucey, J. R., Guzmán, R., Steel, J. & Carter, D. 1997, *MNRAS*, 287, 899
- Nusser, A., da Costa, L. N., Branchini, E., Bernardi, M., Alonso, M. V., Wegner, G., Willmer, C. N. A., & Pellegrini, P. S. 2001, *MNRAS*, 320, 21
- Ramella, M., Geller, M. J., & Huchra, J. P. 1989, *ApJ*, 344, 57
- Saglia, R. P., Colless, M., Burstein, D., Davies, R. L., McMahan, R. K., Wegner, G. 2001, *MNRAS*, 324, 389
- Scodreggio, M. 1997, PhD Thesis, Cornell University
- Scodreggio, M., Giovanelli, R. & Haynes, M. P. 1997, *AJ*, 113, 101
- Scodreggio, M., Gavazzi, G., Belsole, E., Pierini, D., & Boselli, A. 1998, *MNRAS*, 301, 1001
- Smith, R. J., Lucey, J. R., Hudson, M. J. & Steel, J. 1997, *MNRAS*, 291, 461

Sodré, L. Jr. & Lahav, O. 1993, MNRAS, 260, 285

Strauss, M.A. & Willick, J. A. 1995, Physics Reports, 261, 271

Wegner, G., Colless, M., Baggle, G., Davies, R.L., Bertschinger, E., Burstein, D., McMahan, R.K., & Saglia, R.P. 1996, ApJS, 106, 1

Wegner, G., Willmer, C. N. A., Bernardi, M. et al., 2001, in preparation

Willick, J. A. 1994, ApJS, 92, 1

Zaroubi, S., Bernardi, M., da Costa, L. N., Hoffman, Y., Alonso, M. V., Wegner, G., Willmer, C. N. A., & Pellegrini, P. S. 2001, MNRAS, 326, 375

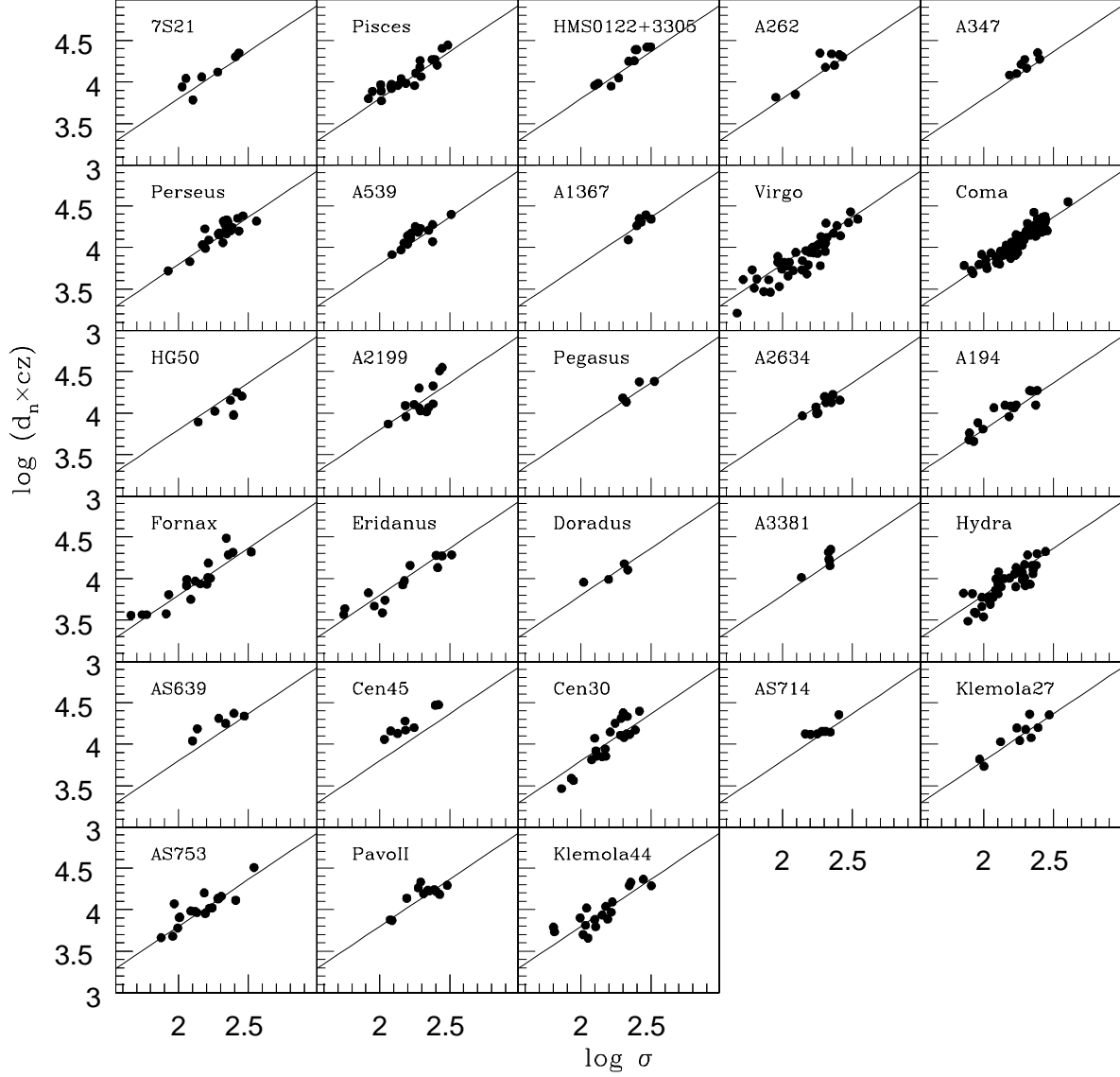


Fig. 1.— The product of  $d_n$  (in 0.1 arcmin) and the redshift (in  $\text{kms}^{-1}$ ) of each cluster galaxy is plotted versus its velocity dispersion. The solid line represents the best fit after minimizing the  $\chi^2$  defined in equation (3) for the first time.

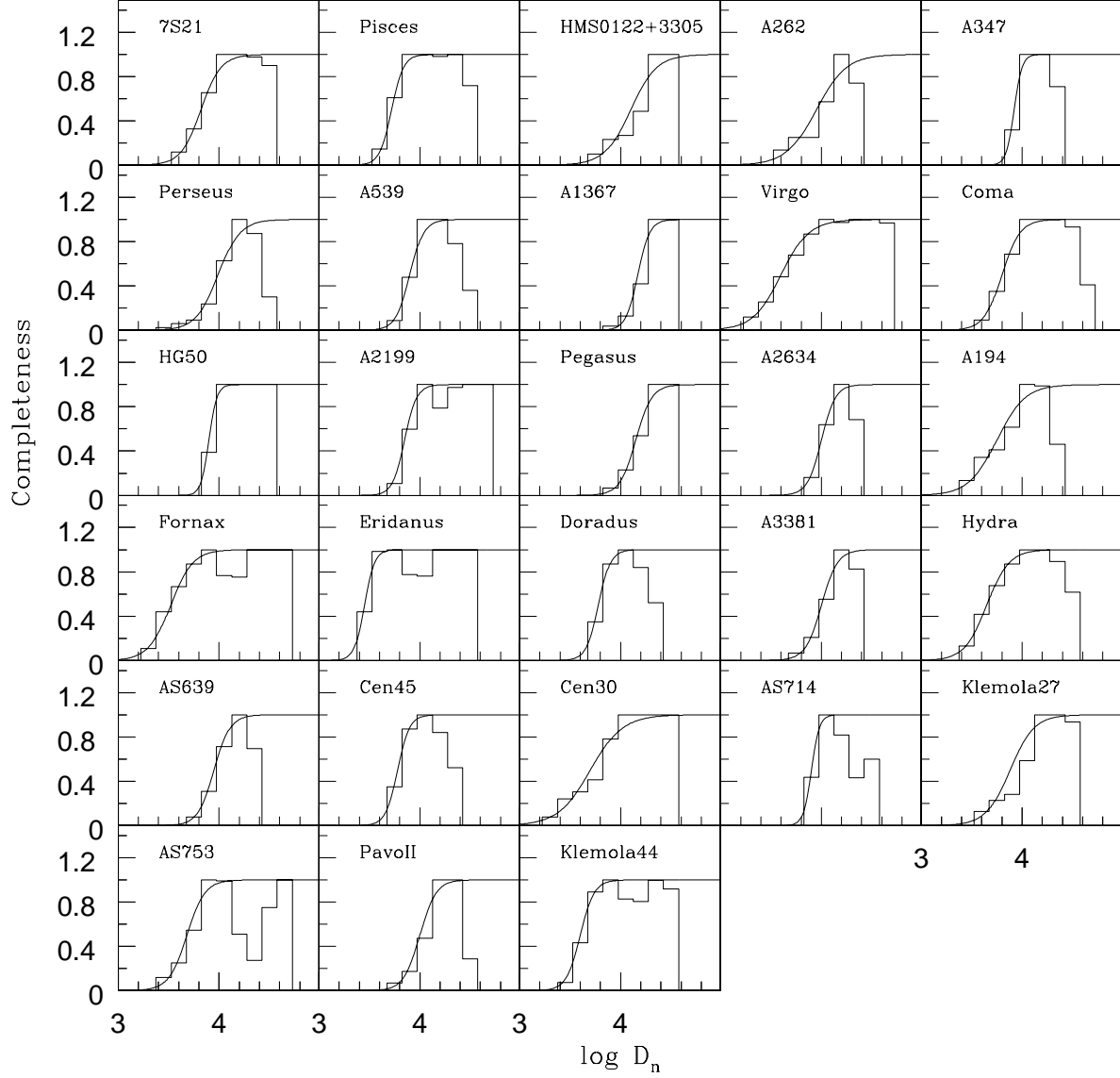


Fig. 2.— Panels show the selection function for each cluster, computed from the ratio of the number of objects observed in the cluster and the number predicted by the fitted diameter distribution function. Solid curves show fits to the histograms of the form given by Equation (8).

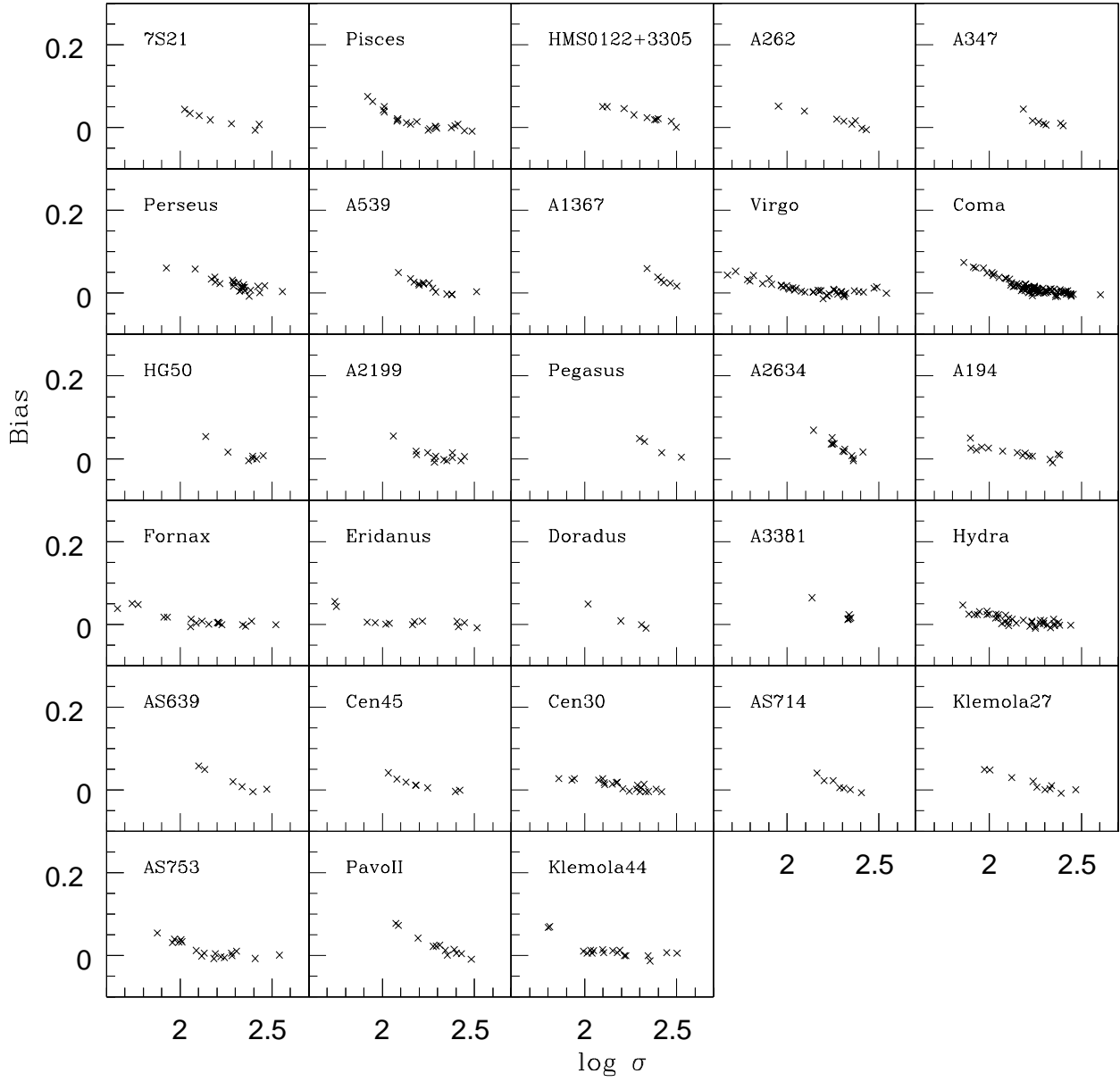


Fig. 3.— The incompleteness bias corrections that were applied to the individual measurements.

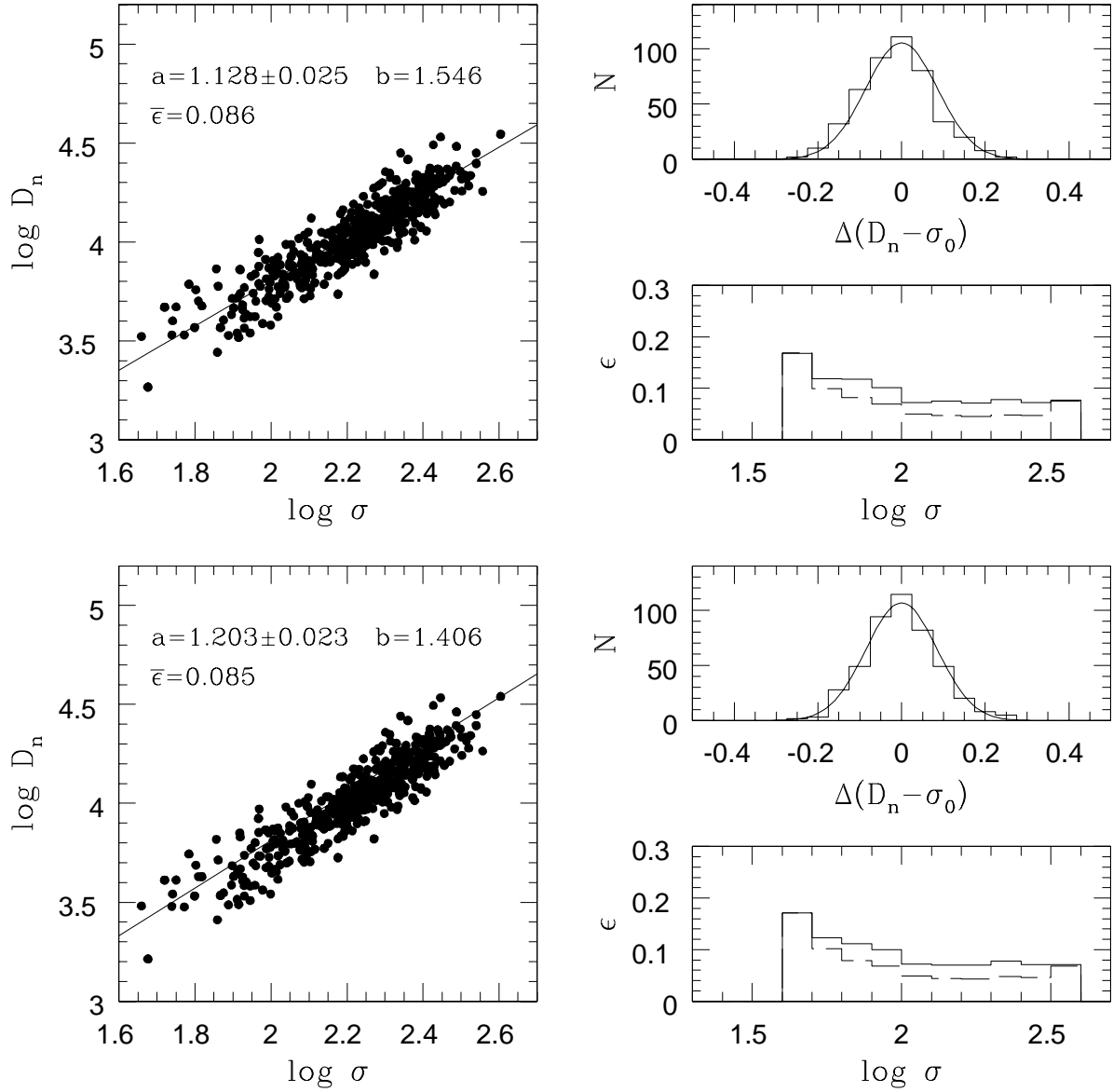


Fig. 4.— Panels on the left show measurements before the bias correction is applied (upper), and the final corrected values derived from the iterative process (lower) as a function of  $\sigma$ . The line shows the derived distance relation. The values of the slope ( $a$ ), zero-point ( $b$ ), and the mean  $rms$  scatter ( $\bar{\epsilon}$ ) are also shown. Panels on the right show the distribution of the residuals relative to the  $D_n - \sigma$  relation, as well as the distribution of the corresponding observed scatter (solid line) and intrinsic scatter (dashed line) as a function of  $\sigma$ .



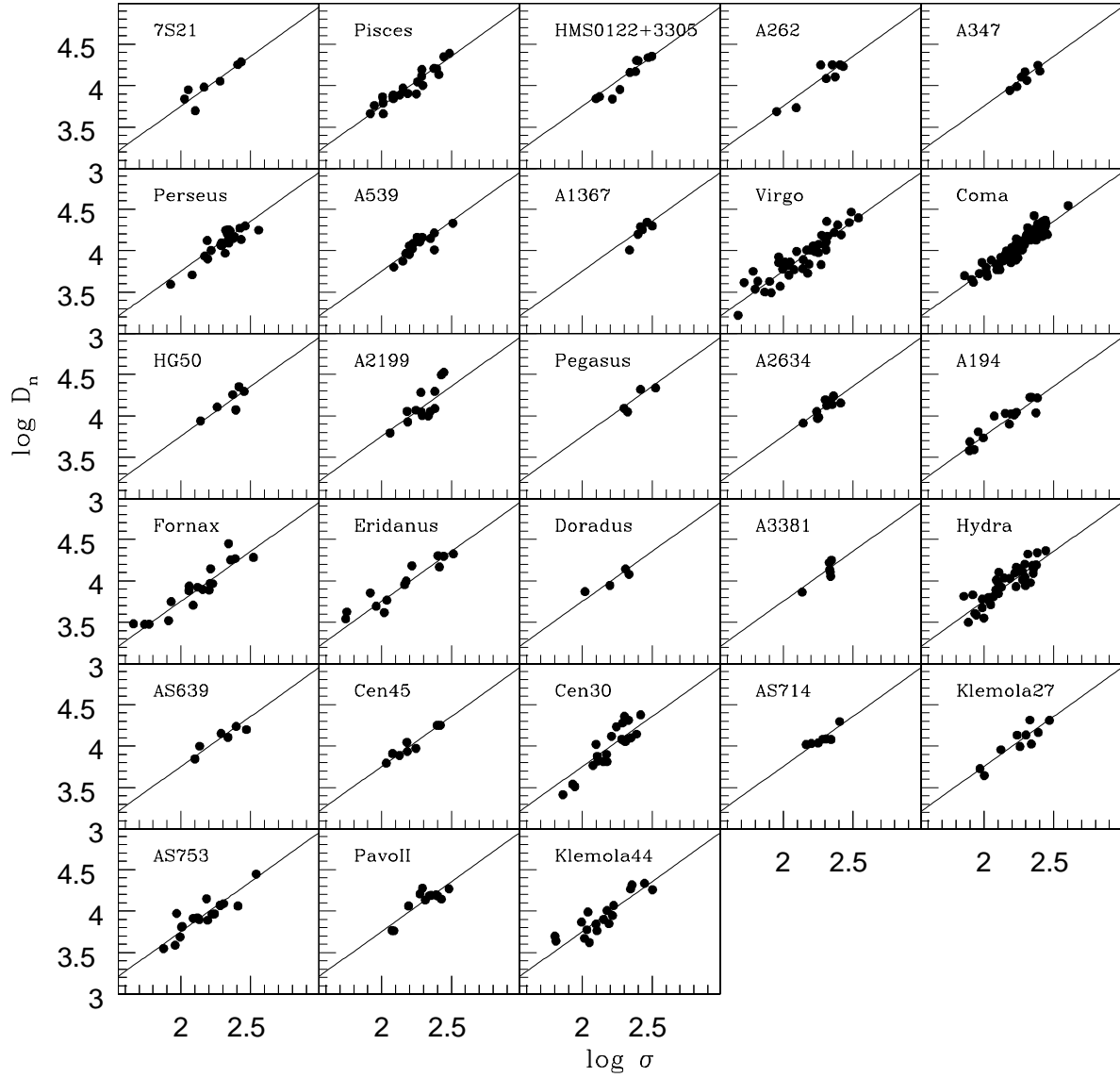


Fig. 5.— Bias-corrected  $D_n$  of each cluster member galaxy versus its velocity dispersion. Solid line shows the derived distance relation (Equation (9)).

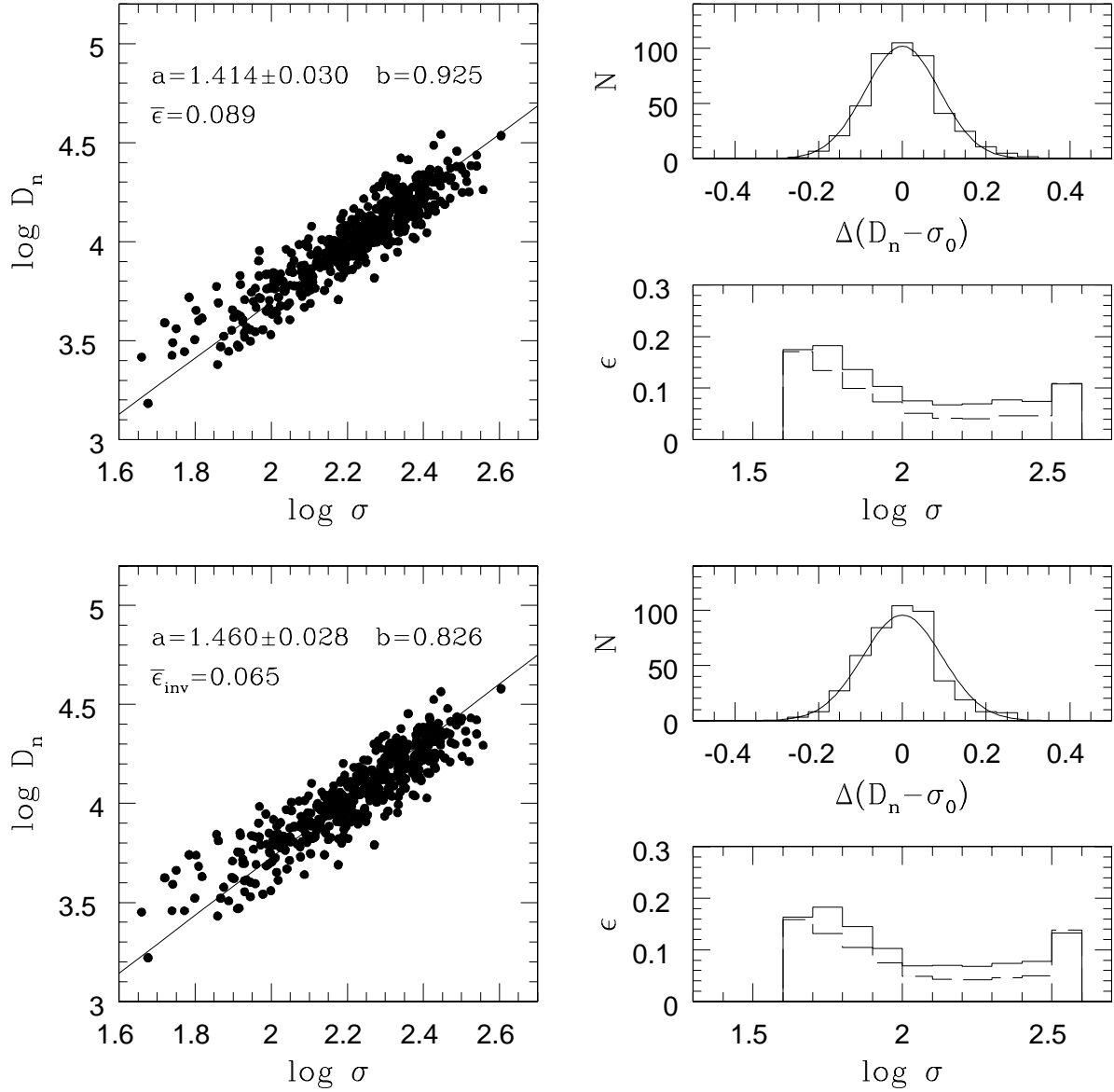


Fig. 6.— Symbols in the panels on the left show the bias corrected measurements; straight lines show the derived bivariate distance relation (upper) and the inverse relation (lower). The values of the slope ( $a$ ), zero-point ( $b$ ), and the mean *rms* scatter ( $\bar{\epsilon}$ ) are also shown. Panels on the right show the distribution of residuals relative to the  $D_n - \sigma$  relation, together with the distribution of the corresponding observed scatter (solid line) and intrinsic scatter (dashed line), as a function of  $\sigma$ .

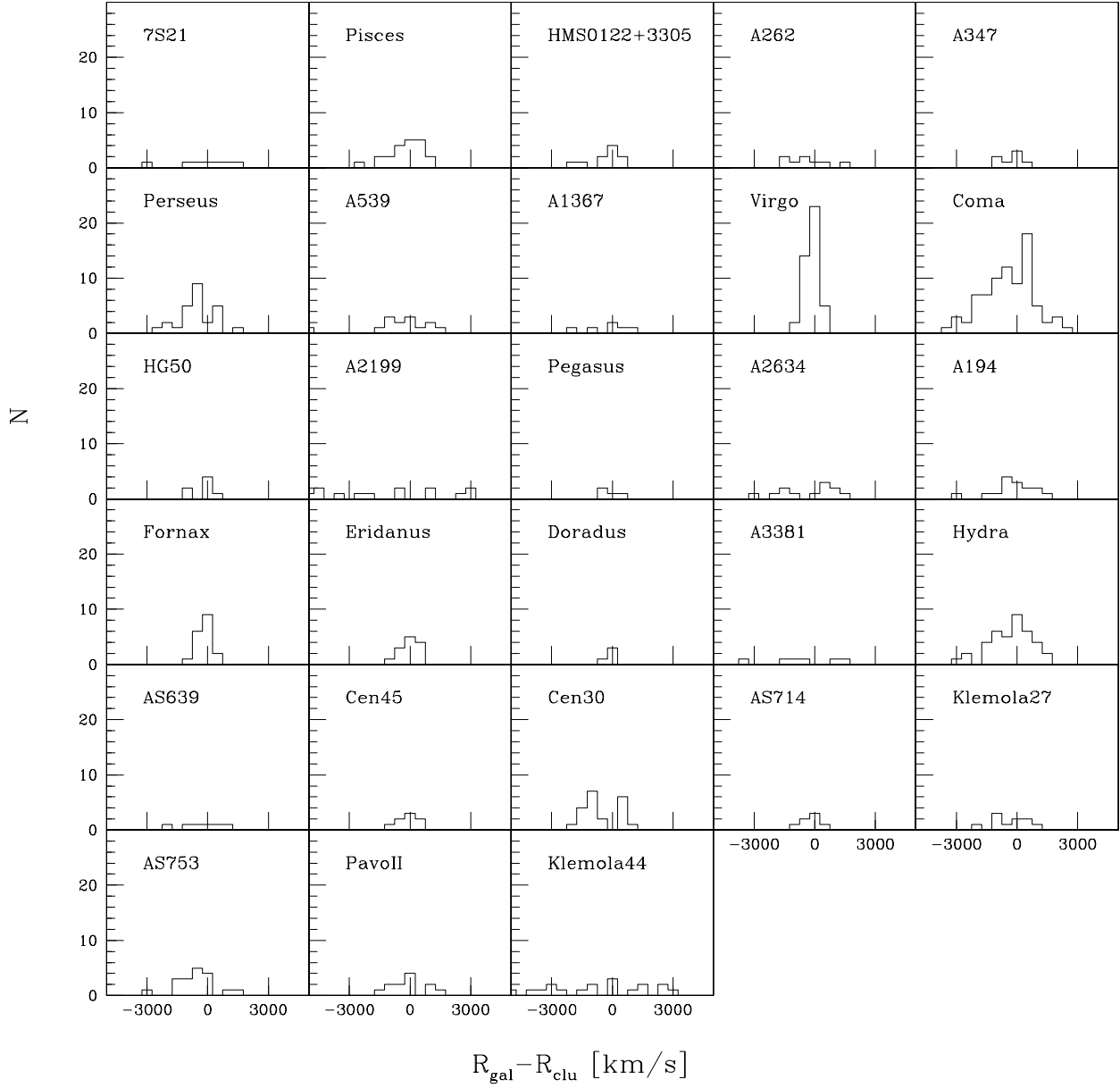


Fig. 7.— The distribution of the difference between the individual galaxy distances derived from Equation( 9), and the error-weighted mean of the distribution, which is used as the cluster distance.

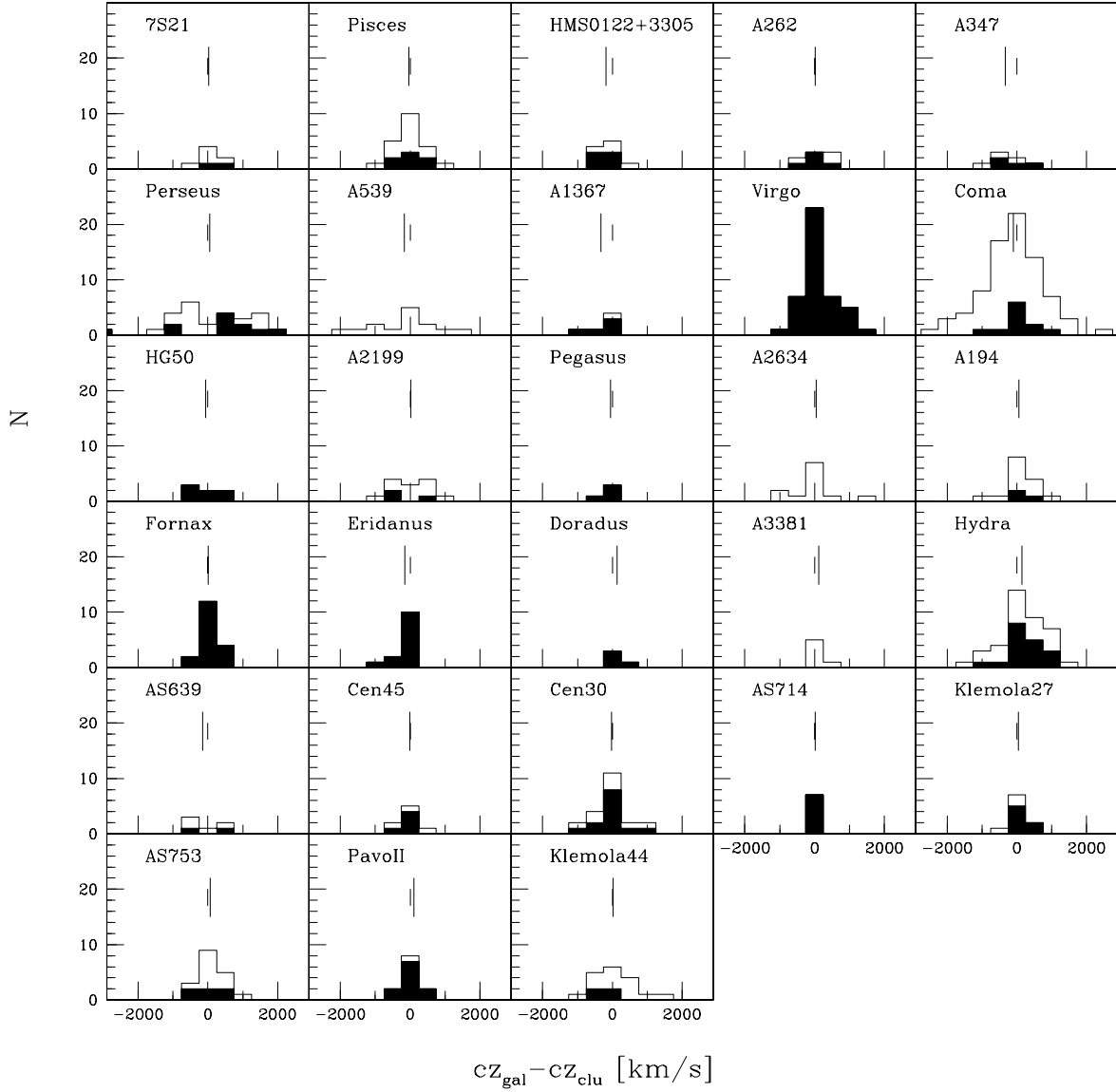


Fig. 8.— The distribution of differences between the galaxy redshifts and that of the cluster to which they were assigned. Open histograms show this distribution for all the galaxies in the cluster, regardless of their apparent magnitude. Solid histograms show the distribution for only those galaxies which were identified as members of the parent cluster by applying an objective group-finding algorithm to complete, magnitude-limited redshift surveys.

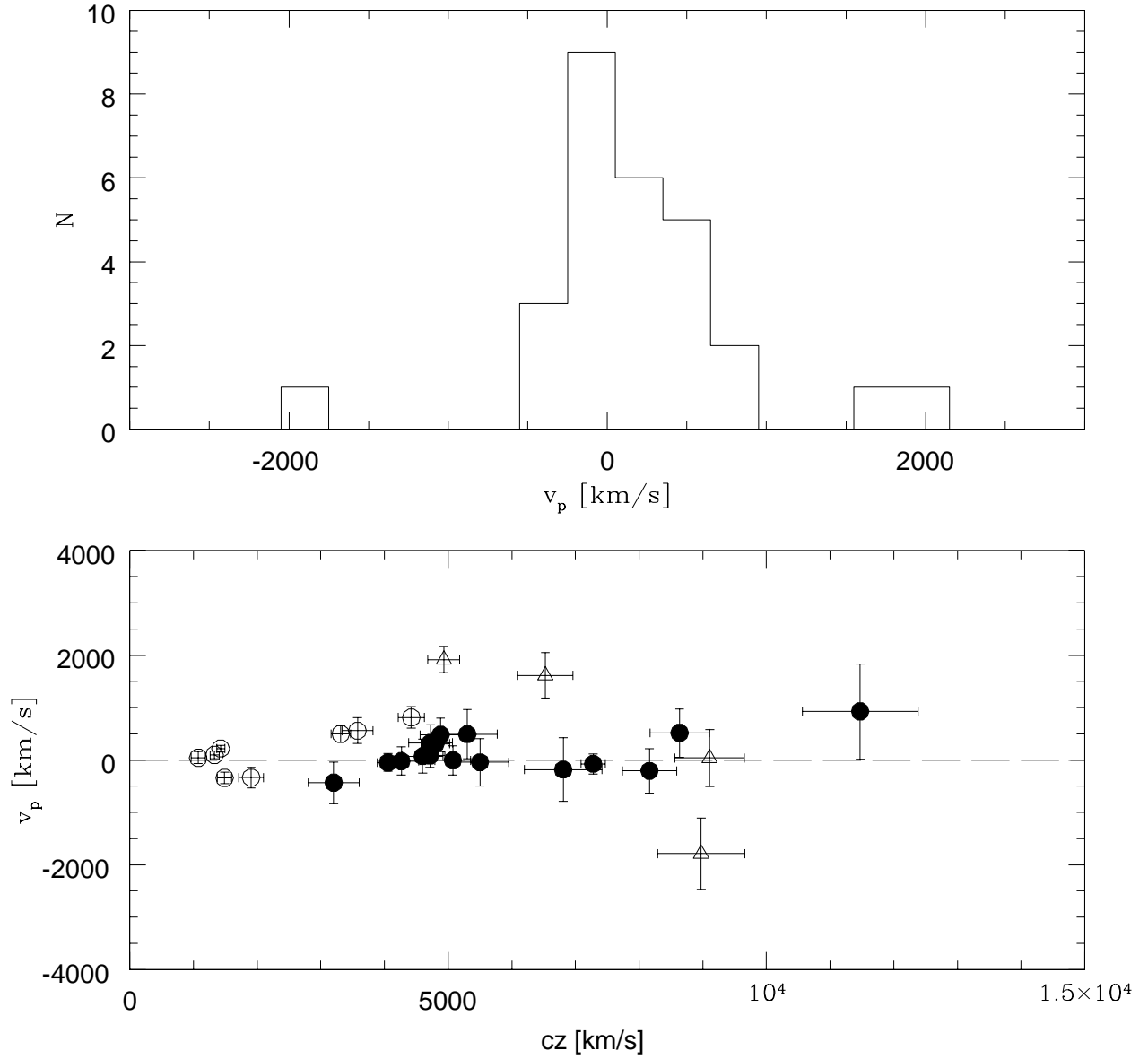


Fig. 9.— Distribution of cluster peculiar velocities (upper panel) and cluster peculiar velocities versus the estimated distances (lower panel). Filled circles represent the “distant” clusters used for the final calibration of the  $D_n - \sigma$  relation; open circles represent either nearby clusters or clusters which have suspiciously large peculiar velocities; and open triangles indicate clusters that were not observed by our survey.

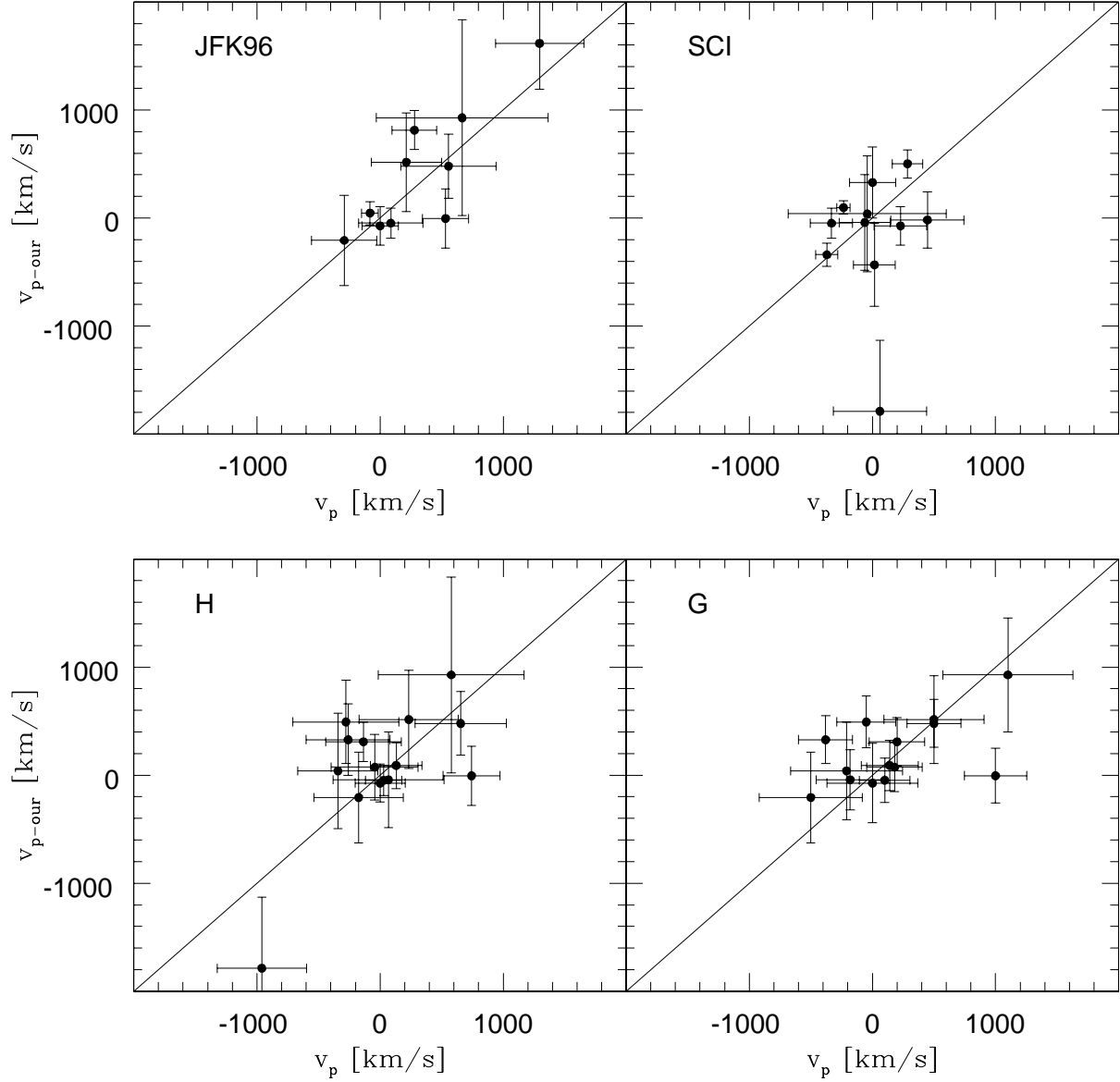


Fig. 10.— Cluster peculiar velocities obtained using Equation (9) versus the values computed by Jørgensen et al. (1996) (JFK96), Giovanelli et al. (1997) (SCI), Hudson et al. (1997) (H), and Gibbons et al. (1998) (G).

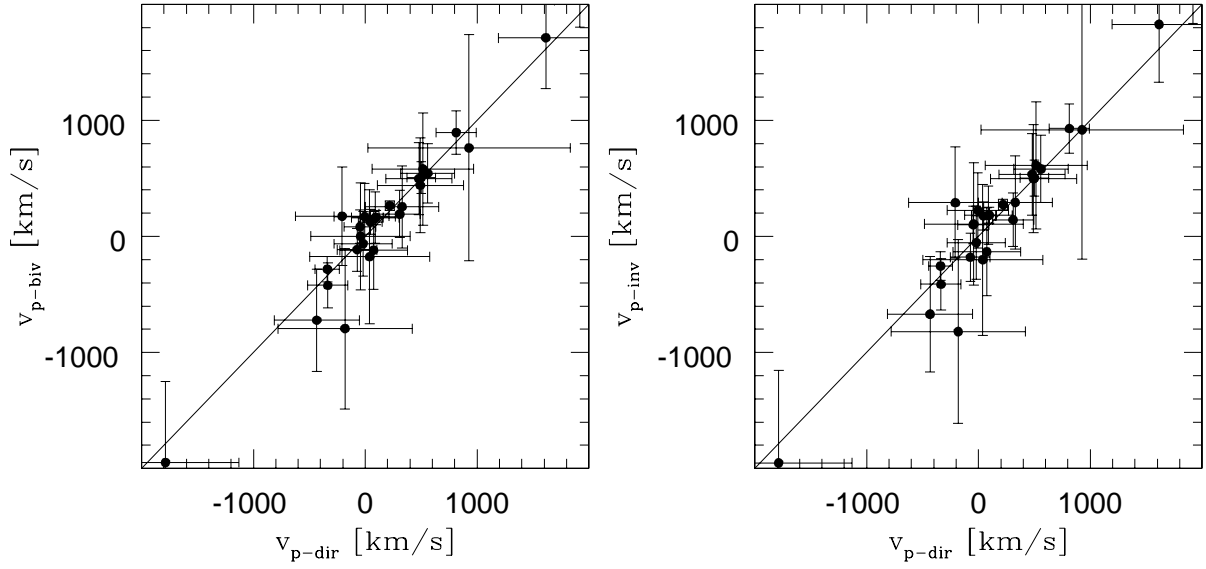


Fig. 11.— Cluster peculiar velocities obtained using the direct  $D_n - \sigma$  relation (Equation (9)) versus the values computed using the bivariate (left) and the inverse relations (right).

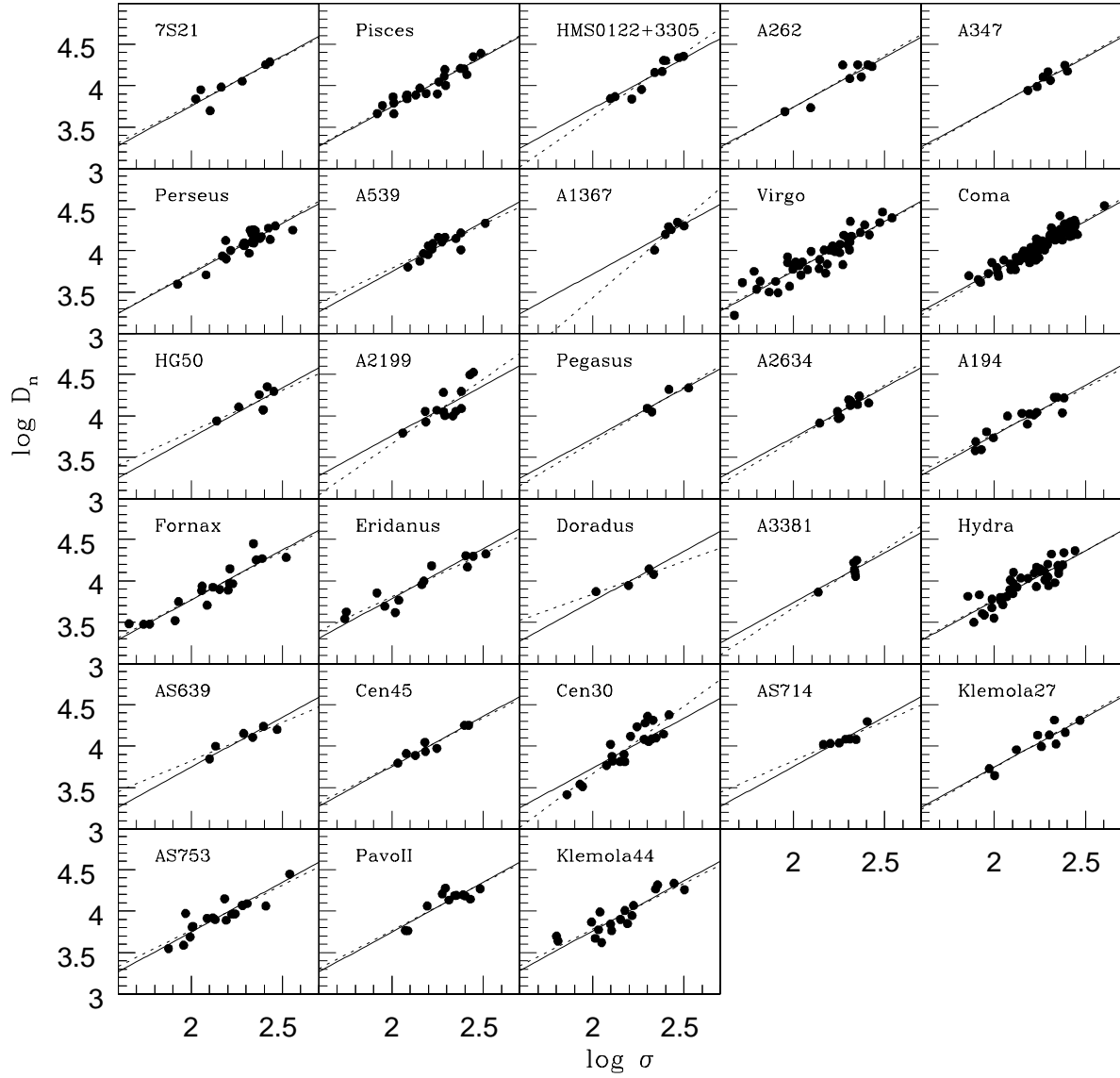


Fig. 12.— The individual cluster  $D_n - \sigma$  relations obtained by fitting the bias-corrected data points of the cluster (dashed line). The solid line in all panels shows the template distance relation given by Equation (9).



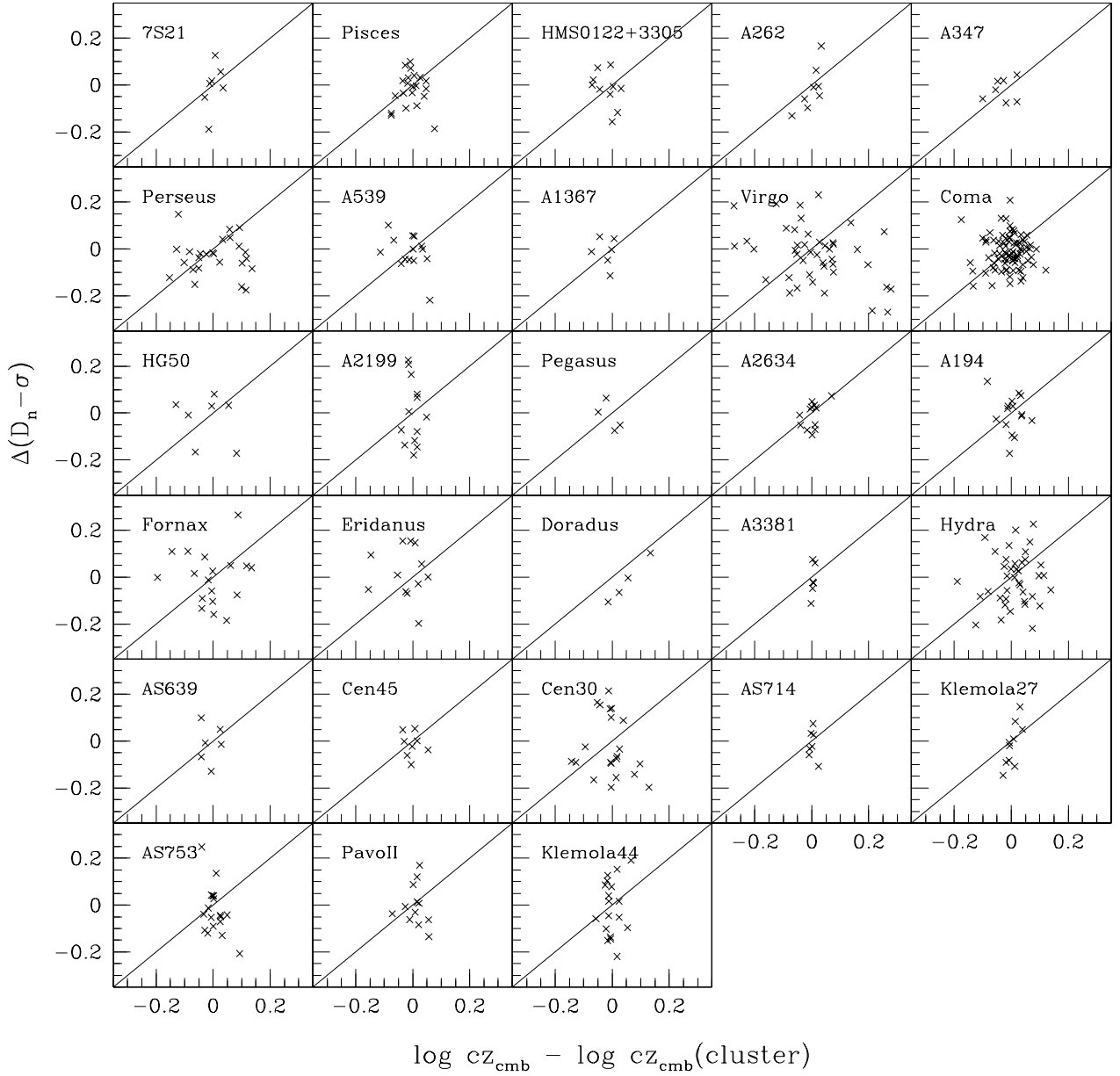


Fig. 13.— The residual, relative to the distance relation, of each galaxy, as a function of the difference between the galaxy’s redshift and that adopted for its parent cluster.

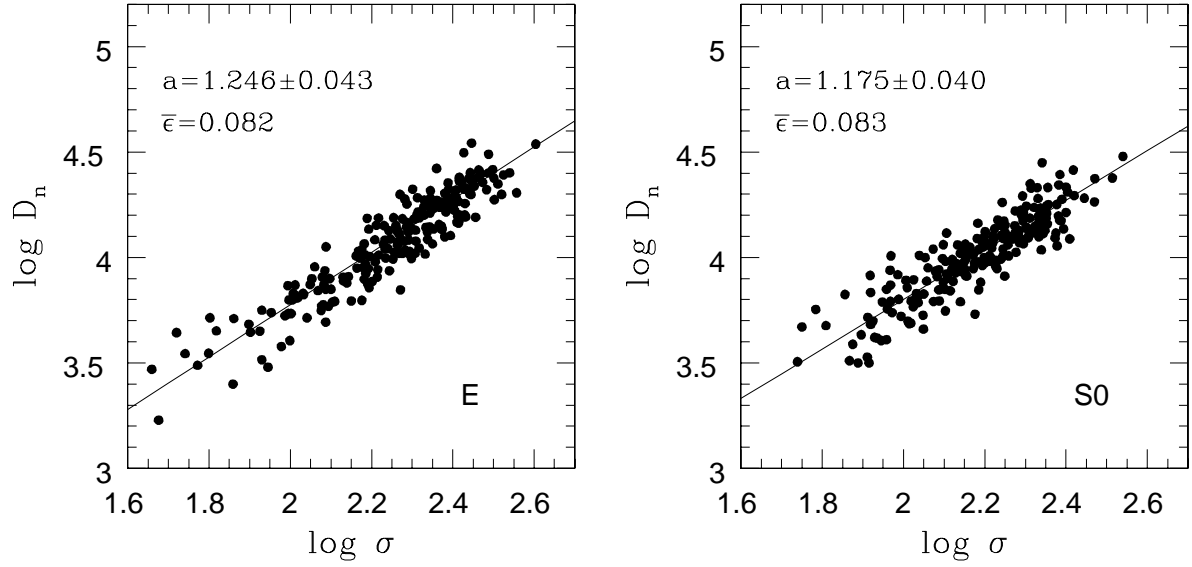


Fig. 14.— The  $D_n - \sigma$  relation obtained from ellipticals (left panel) and S0s (right panel). The slope ( $a$ ) of the relation and the corresponding mean  $rms$  scatter ( $\bar{\epsilon}$ ) are also shown.

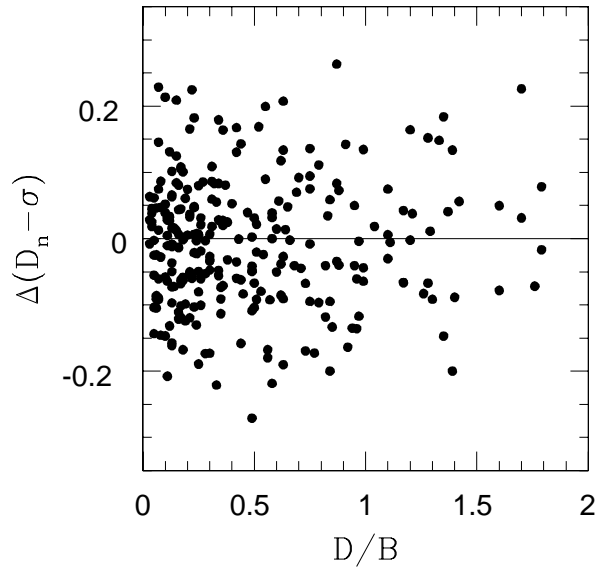


Fig. 15.— The residuals, relative to the distance relation, as a function of the galaxy  $D/B$  ratio.

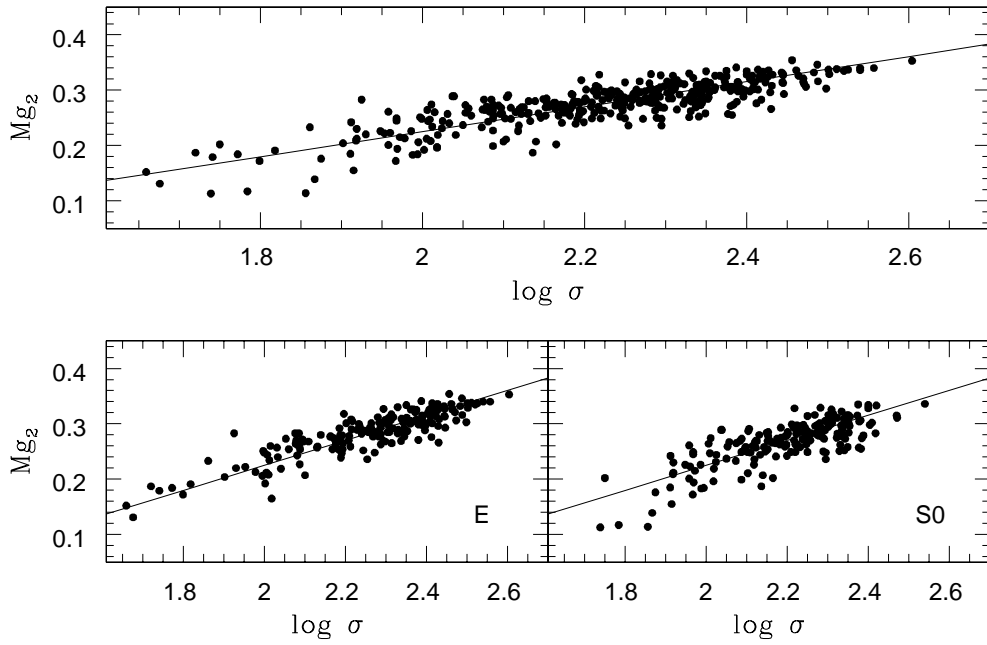


Fig. 16.— (Upper panel) Measurements of the  $Mg_2$  index versus the velocity dispersion for the whole cluster sample. The solid line is the  $Mg_2 - \sigma$  relation derived from the bivariate fit. (Lower panels) As in the upper panel, but here the sample is split into ellipticals (left) and S0s (right). In both lower panels, the solid line has the same slope as in the upper panel (for the whole sample) while the zero-point has changed.

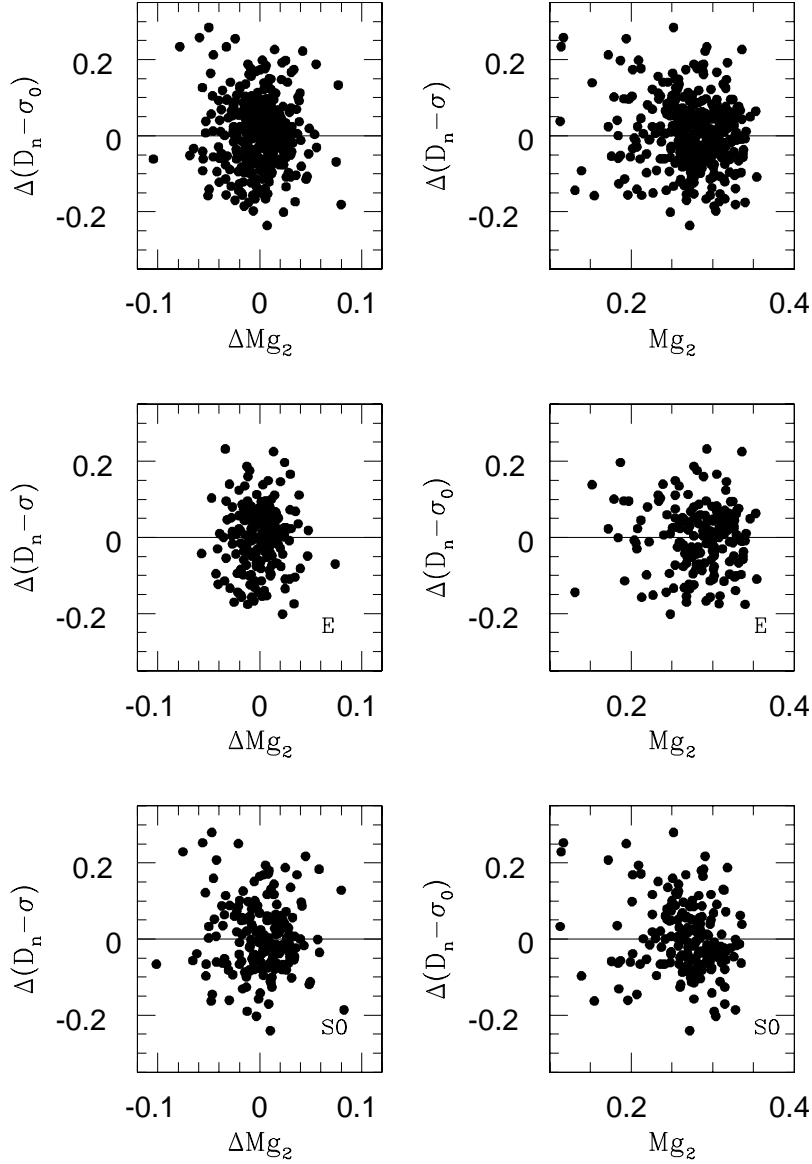


Fig. 17.— (Left panels) Residuals with respect to the mean  $D_n - \sigma$  relation versus residuals with respect to the mean  $Mg_2 - \sigma$  relation for the cluster sample as a whole (upper panel), for the ellipticals (middle panel), and for S0s (lower panel). (Right panels) As on the left, but now for the residuals of the  $D_n - \sigma$  relation versus the measured  $Mg_2$  index.

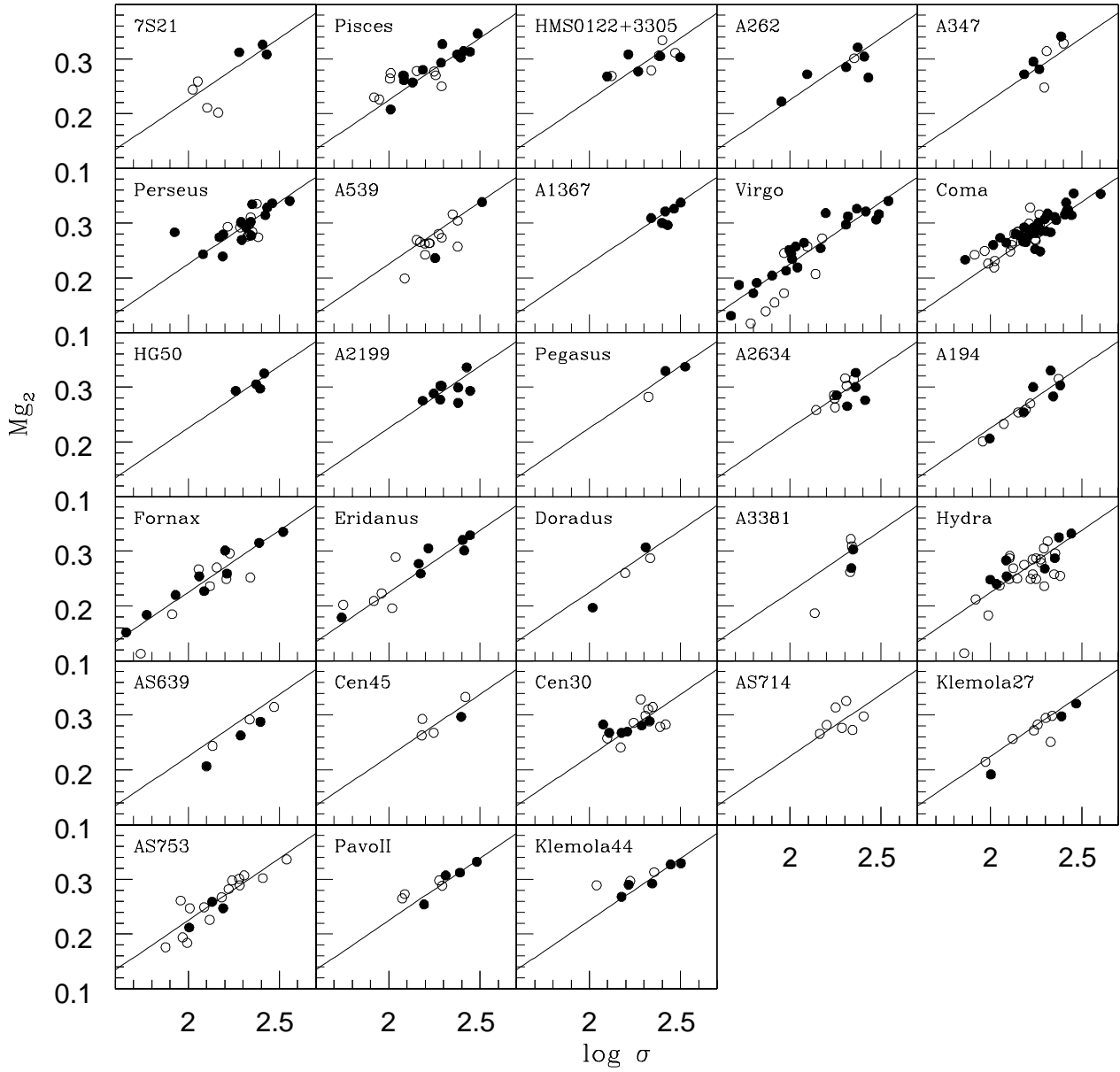


Fig. 18.— The  $Mg_2$  index of each cluster member galaxy versus its velocity dispersion. Open circles indicate SO galaxies while filled circles ellipticals. Solid line shows the derived composite  $Mg_2 - \sigma$  relation.

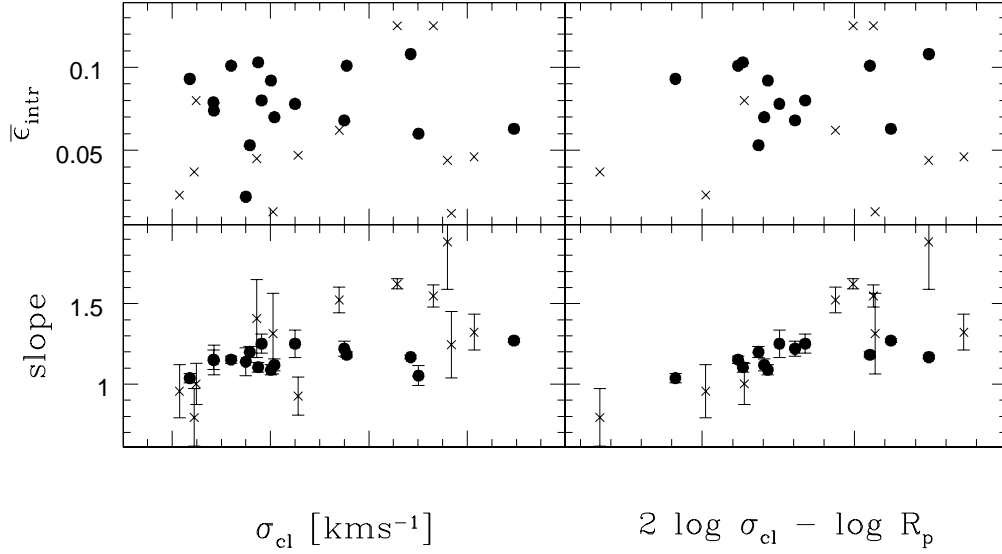


Fig. 19.— The *rms* scatter (upper panels) and the slope (bottom panels) of the individual cluster  $D_n - \sigma$  relations versus: (left panels) the measured velocity dispersion of the cluster  $\sigma_{cl}$ ; and (right panels) the logarithm of the ratio  $\sigma_{cl}^2/R_p$ , where  $R_p$  is the pair radius defined by Ramella et al.(1989). Seven clusters taken from the literature, which were not identified by the finding algorithm, are not included in the right panels of the figure. (Crosses) clusters/groups with a large error in the slope ( $\gtrsim 0.1$ ; see Table reftab:clusindiv) or which exhibit clear evidence of either spatial sub-structure or distinct galaxy populations (HMS0122+3305, A2199, Cen30); (filled circles) clusters/groups with reliable  $D_n - \sigma$  fits.

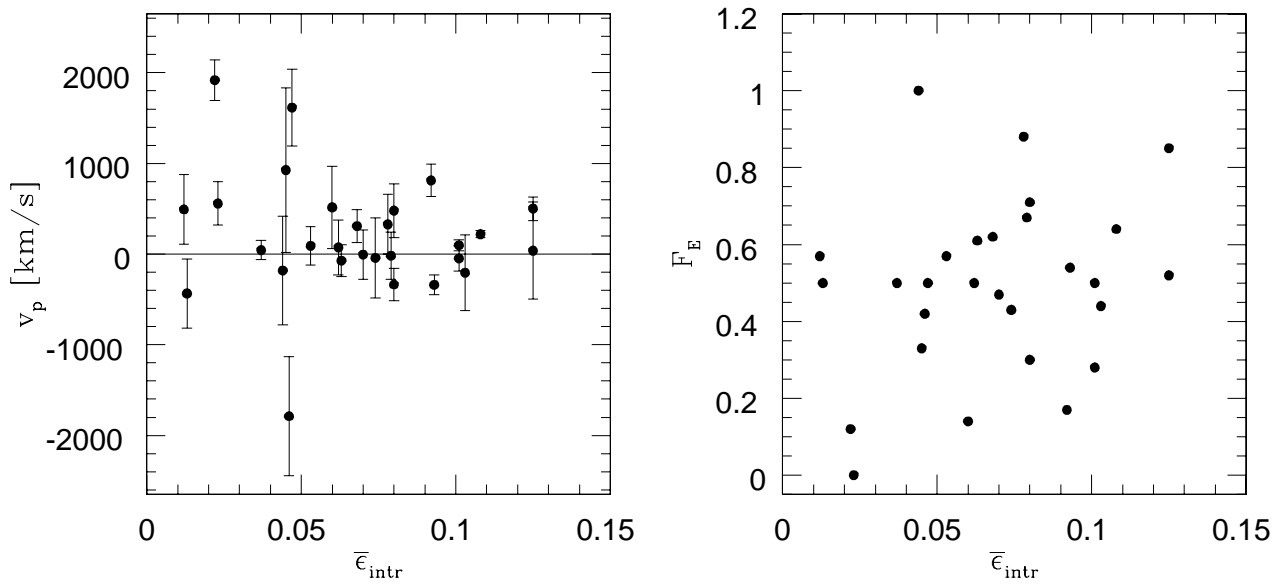


Fig. 20.— Left panel: peculiar velocities of the 28 clusters as a function of the amplitude of the scatter of the individual  $D_n - \sigma$  relations of each cluster. Right panel: the fraction of elliptical to early-type galaxies  $F_E = (N_E/(N_E + N_{S0}))$ , for each cluster, versus the scatter of the individual  $D_n - \sigma$  relations.



Table 1: Completeness function coefficients

Cluster Name (1)	$y_f$ (2)	$\eta$ (3)
7S21	3.82	0.10
Pisces	3.72	0.06
HMS0122+3305	4.10	0.13
A262	3.95	0.15
A347	3.92	0.04
Perseus	3.99	0.11
A539	3.90	0.07
A1367	4.17	0.06
Virgo	3.60	0.14
Coma	3.80	0.09
HG50	3.90	0.04
A2199	3.85	0.06
Pegasus	4.15	0.08
A2634	4.00	0.07
A194	3.75	0.14
Fornax	3.52	0.11
Eridanus	3.45	0.05
Doradus	3.78	0.06
A3381	4.00	0.06
Hydra	3.65	0.11
AS639	3.95	0.08
Cen45	3.78	0.06
Cen30	3.70	0.16
AS714	3.90	0.04
Klemola27	3.88	0.12
AS753	3.68	0.09
PavoII	4.00	0.08
Klemola44	3.60	0.07

Table 2: Tests of the  $D_n - \sigma$  relation

Objects removed	$N_{\text{remain}}$	$a$	$b$	$\bar{\epsilon}$
(1)	(2)	(3)	(4)	(5)
A <sup>1</sup>	360	1.197	1.423	0.084
B <sup>2</sup>	374	1.184	1.448	0.086
7S21	447	1.204	1.405	0.083
Pisces	433	1.202	1.407	0.084
HMS0122+3305	444	1.199	1.413	0.083
A262	446	1.204	1.406	0.083
A347	447	1.203	1.407	0.083
Perseus	428	1.202	1.411	0.084
A539	440	1.203	1.406	0.083
A1367	448	1.203	1.407	0.083
Virgo	410	1.203	1.408	0.079
Coma	374	1.187	1.438	0.086
HG50	447	1.203	1.405	0.083
A2199	441	1.194	1.424	0.081
Pegasus	450	1.204	1.405	0.083
A2634	442	1.202	1.408	0.083
A194	439	1.206	1.400	0.083
Fornax	436	1.206	1.401	0.082
Eridanus	441	1.209	1.397	0.082
Doradus	450	1.202	1.408	0.083
A3381	448	1.202	1.408	0.083
Hydra	415	1.204	1.404	0.081
AS639	448	1.203	1.407	0.083
Cen45	446	1.203	1.408	0.083
Cen30	433	1.183	1.448	0.080
AS714	447	1.203	1.407	0.083
Klemola27	444	1.203	1.408	0.083
AS753	436	1.205	1.403	0.082
PavoII	442	1.201	1.412	0.083
Klemola44	436	1.204	1.406	0.082

Notes. — (1) peripheral cluster galaxies; (2) clusters whose individual  $D_n - \sigma$  relations differ significantly ( $\Delta$  slope  $\gtrsim 0.2$ ) from equation (9): HMS0122+3305, A1367, HG50, A2199, Doradus, A3381, AS639, Cen30, and AS714.

Table 3: Our determinations of the  $D_n - \sigma$  relation

Type	$a$	$b$	$\bar{\epsilon}$	note
(1)	(2)	(3)	(4)	(5)
direct	$1.203 \pm 0.023$	1.406	0.085	
direct orthogonal fit	$1.414 \pm 0.030$	0.925	0.089	
inverse	$1.460 \pm 0.028$	0.826	0.075	1

Notes. — (1) the uncertainty in the distances determined using the inverse relation is ( $a \times \bar{\epsilon}$ ).

Table 4: Other determinations of the  $D_n - \sigma$  relation

Source	Type	$a$	$b$	$\bar{\epsilon}$	note
(1)	(2)	(3)	(4)	(5)	(6)
LC	direct	$1.200 \pm$	-1.679	0.090	1
7S	direct	$1.200 \pm$	1.411	0.090	
D	direct	$1.330 \pm$	-1.967	0.110	1
B96	direct	$0.938 \pm 0.072$	-	0.071	
JFK96	orthogonal	$1.320 \pm 0.070$	-	0.088	
Lc	direct	$0.913 \pm 0.090$	-1.019	0.075	1
DCZC97	direct	$1.240 \pm 0.060$	-1.080	0.080	2
HLSS97	inverse	$1.419 \pm 0.044$	-	0.065	3
GFB	inverse	$1.420 \pm 0.040$	-	0.059	3

References. — LC: Lucey & Carter (1988); 7S: Lynden-Bell et al. (1988); D: Dressler et al. (1991); B96: Bagglely (1996); JFK96 : Jorgensen et al. (1996); Lc: Lucey et al. (1997); DCZC97: D’Onofrio et al. (1997); HLSS97 : Hudson et al. (1997); GFB: Gibbons et al. (1998).

Notes. — (1) they used  $\log D_n = a \log \sigma + b$  with  $D_n$  in arcsec. Using  $D_n = \log(d_n \times R)$ , where  $d_n$  is in 0.1 arcmin, one must add  $\log R_{\text{Coma}} - 0.778$  to their zero point. (2) as in (1), but substitute  $R_{\text{Coma}}$  for  $R_{\text{Virgo}}$ . (3) the uncertainty in the distances determined using the inverse relation is ( $a \times \bar{\epsilon}$ ).

Table 5: Clusters distance and peculiar velocity

Name (1)	$n_{gal}$ (2)	l (3)	b (4)	$cz^{CMB}$ (5)	R (6)	$v_{pec}^{CMB}$ (7)
7S21	7	113.784	-40.018	5500±90	5542±441	-41±451
Pisces	21	127.243	-30.185	4715±89	4626±213	89±231
HMS0122+3305	10	130.513	-28.767	4600±108	4525±301	74±320
A262	8	136.599	-25.049	4725±93	4396±328	328±341
A347	7	141.124	-17.896	5301±111	4808±383	492±398
Perseus	26	150.382	-13.382	4799±133	4490±185	309±228
A539	14	195.698	-17.717	8636±75	8119±457	516±464
A1367	6	234.292	73.052	6807±94	6989±602	-181±609
Virgo	44	283.871	74.200	1427±49	1208±38	219±62
Coma	80	58.301	88.285	7278±75	7351±173	-72±189
HG50	7	0.458	49.270	1905±83	2240±178	-334±197
A2199	13	62.885	43.906	9108±111	9069±530	39±542
Pegasus	4	87.892	-48.241	3202±108	3635±383	-433±398
A2634	12	103.402	-33.161	8975±112	10762±655	-1787±664
A194	15	142.860	-62.908	5074±60	5079±276	-5±283
Fornax	18	236.241	-54.096	1330±36	1234±61	96±71
Eridanus	13	212.165	-51.577	1488±28	1827±106	-339±110
Doradus	4	260.209	-47.227	1073±36	1028±108	45±114
A3381	6	240.293	-22.697	11472±65	10544±908	927±910
Hydra	39	269.707	26.334	4055±95	4103±138	-47±168
AS639	6	280.534	10.908	6526±93	4910±423	1615±433
Cen45	8	302.553	21.659	4931±110	3013±224	1918±250
Cen30	21	302.023	21.852	3313±82	2812±129	500±153
AS714	7	302.802	36.309	3576±49	3017±240	559±245
Klemola27	10	317.338	30.639	4881±102	4402±293	479±310
AS753	18	319.166	26.744	4421±97	3608±179	812±204
PavoII	12	332.191	-23.755	4266±63	4285±261	-18±268
Klemola44	18	25.336	-75.807	8162±88	8369±416	-206±425

Notes. — See Appendix A.

Table 6: Individual cluster  $D_n - \sigma$  relations

Cluster (1)	$N_{\text{gal}}$ (2)	$a$ (3)	$\bar{\epsilon}$ (4)	$\Delta b$ (5)	$\bar{\epsilon}_{\Delta}$ (6)	$\bar{\epsilon}_{\text{intr}}$ (7)	$F_E$ (8)
7S21	7	1.150±0.093	0.089	0.001	0.090	0.074	0.43
Pisces	21	1.200±0.035	0.069	-0.006	0.068	0.053	0.57
HMS0122+3305	10	1.523±0.080	0.065	-0.028	0.074	0.062	0.50
A262	8	1.251±0.085	0.089	-0.013	0.090	0.078	0.88
A347	7	1.246±0.206	0.046	-0.013	0.045	0.012	0.57
Perseus	26	1.220±0.047	0.082	-0.027	0.080	0.068	0.62
A539	14	1.053±0.062	0.071	-0.007	0.072	0.060	0.14
A1367	6	1.883±0.295	0.053	-0.034	0.063	0.044	1.00
Virgo	44	1.168±0.011	0.115	0.000	0.115	0.108	0.64
Coma	80	1.271±0.012	0.071	-0.002	0.071	0.063	0.61
HG50	7	1.002±0.127	0.091	-0.018	0.093	0.080	0.71
A2199	13	1.549±0.069	0.125	0.006	0.131	0.125	0.85
Pegasus	4	1.315±0.251	0.057	-0.027	0.058	0.013	0.50
A2634	12	1.323±0.112	0.058	-0.014	0.058	0.046	0.42
A194	15	1.120±0.038	0.079	0.012	0.080	0.070	0.47
Fornax	18	1.153±0.022	0.108	0.017	0.108	0.101	0.50
Eridanus	13	1.038±0.029	0.093	0.035	0.101	0.093	0.54
Doradus	4	0.793±0.179	0.042	0.001	0.066	0.037	0.50
A3381	6	1.408±0.242	0.065	-0.016	0.067	0.045	0.33
Hydra	39	1.183±0.017	0.108	0.009	0.108	0.101	0.28
AS639	6	0.927±0.118	0.055	-0.009	0.068	0.047	0.50
Cen45	8	1.140±0.086	0.047	0.001	0.047	0.022	0.12
Cen30	21	1.623±0.031	0.111	-0.019	0.130	0.125	0.52
AS714	7	0.956±0.166	0.048	-0.001	0.051	0.023	0.00
Klemola27	10	1.252±0.060	0.088	-0.009	0.089	0.080	0.30
AS753	18	1.090±0.031	0.097	-0.006	0.100	0.092	0.17
PavoII	12	1.151±0.061	0.086	-0.006	0.086	0.079	0.67
Klemola44	18	1.105±0.030	0.109	0.008	0.111	0.103	0.44

Table 7: Our determination of the  $Mg_2 - \sigma$  relation

Sample	$N_{\text{gal}}$	$a$	$b$	$\bar{\epsilon}$
(1)	(2)	(3)	(4)	(5)
All	369	$0.226 \pm 0.014$	$-0.227 \pm 0.010$	0.021
E	186		$-0.226 \pm 0.014$	0.019
S0	183		$-0.230 \pm 0.015$	0.023